Electronic Supplementary Information (ESI)

Convergent Growth Approach to Redox-Active Ferrocene Rich Carbosilane- and Siloxane-Based Dendrons, Dendrimers and Dendronized Polymers

Sonia Bruña,*,† Josefina Perles‡ and Isabel Cuadrado†

†*Departamento de Química Inorgánica and Institute for Advanced Research in Chemical Sciences (IAdChem), Facultad de Ciencias, Calle Francisco Tomás y Valiente, 7, Universidad Autónoma de Madrid, Ciudad Universitaria de Cantoblanco, 28049, Madrid, Spain.*

‡*Laboratorio de Difracción de Rayos X de Monocristal, Servicio Interdepartamental de Investigación (SIdI), Universidad Autónoma de Madrid, Ciudad Universitaria de Cantoblanco, 28049, Madrid, Spain.*

Correspondence: sonia.brunna@uam.es

CONTENTS

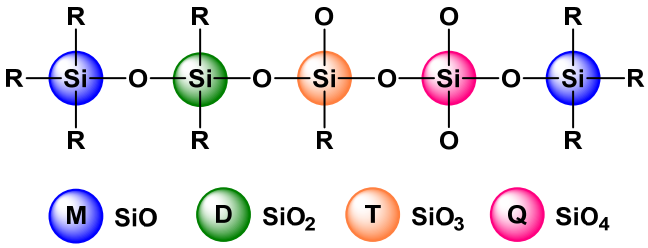

Scheme 1. Terminology used to represent the siloxane structures $R_3SiO_{0.5}$ (M), R_2SiO (D), $RSiO_{1.5}$ (T) and SiO_2 (Q).

1. Synthetic Procedures

Attempts to synthesize dendrimer 6. **G1**-dendron **3** (79 mg, 0.058 mmol) in 5 mL of toluene, Karstedt's catalyst (10 µL), and tetrakis(dimethylsiloxy)silane **I** (4 µL, 0.012 mmol) were used. In the initial attempt, the reaction mixture was stirred for 24 h at 70 °C, while the second one was heated at 100 °C for 72 h. Despite the subsequent precipitation processes, with different mixtures of *n*-hexane/CH_2Cl_2, the desired dendrimer **6** could not be identified so far. Only dendrimers with different structural defects were identified by MALDI-TOF: *m/z* 4450.0 (one unfunctionalized branch ended in a Si–OH group), *m/z* 3080.2 (two unfunctionalized branches, one ended in Si–H and the other in Si–OH), *m/z* 3096.2 (two unfunctionalized branches ended in Si–OH), *m/z* 1726.1 (three unfunctionalized branches, two ended in Si–OH and one in Si–H), *m/z* 1742.1 (three unfunctionalized branches ended in Si–OH).

Note: Most likely, the -Si-OH terminal groups, detected for some of the dendrimers with structural defects, were formed under the reaction conditions tested for the hydrosilylation between dendron **3** and siloxane $Si[OSi(CH_3)_2H]_4$, which implied high temperature and long reaction times. The Si-H groups that were not able to react with dendron **3**, due to its steric hindrance, did react, given enough time, to form the Si-OH groups in the presence of the Karstedt's catalyst and possible oxygen and/or water traces.

We have previously reported that -Si-H bonds can be transformed into -Si-OH bonds at high temperature, in the presence of Karstedt's catalyst (see Crystals 2022, 12, 1122, https://doi.org/10.3390/cryst12081122 and references therein, above all: Macromolecules 2009, 42, 9199–9203 https://doi.org/10.1021/ma9018608).

Attempts to synthesize a second generation dendronized polymer from dendron 3. **G1**-dendron **3** (80 mg, 0.059 mmol), toluene (4 mL), Karstedt's catalyst (10 µL), and poly(methylhydrosiloxane) **II** (3 µL, 0.012 mmol) were used. The reaction mixture was stirred for 45 h at 100 °C and the oily residue obtained was repeatedly dissolved in the minimum amount of CH_2Cl_2 and precipitated into methanol. In this case, isolation of pure dendrimeric compounds from the multicomponent mixtures proved to be a very difficult task.

2. Spectra and analysis of compounds 1-9_n

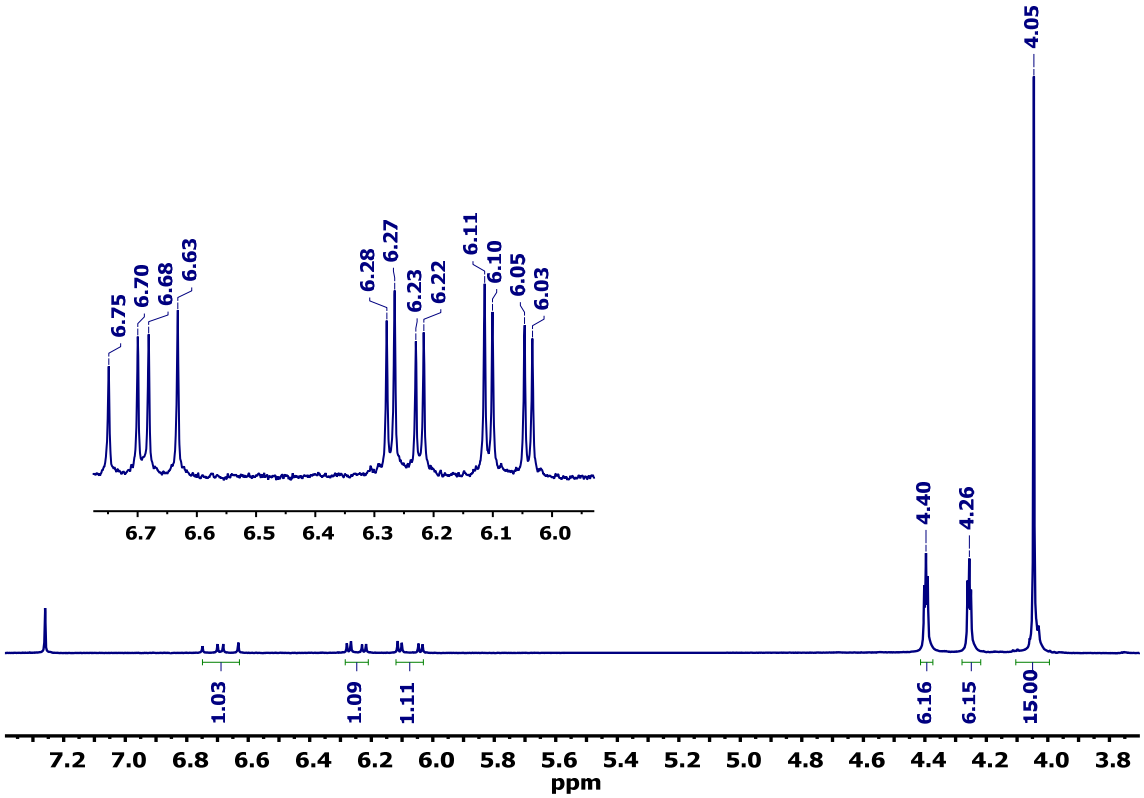

Figure S1: ^{1}H NMR spectrum of triferrocenylvinylsilane **1** (300 MHz, $CDCl_3$).

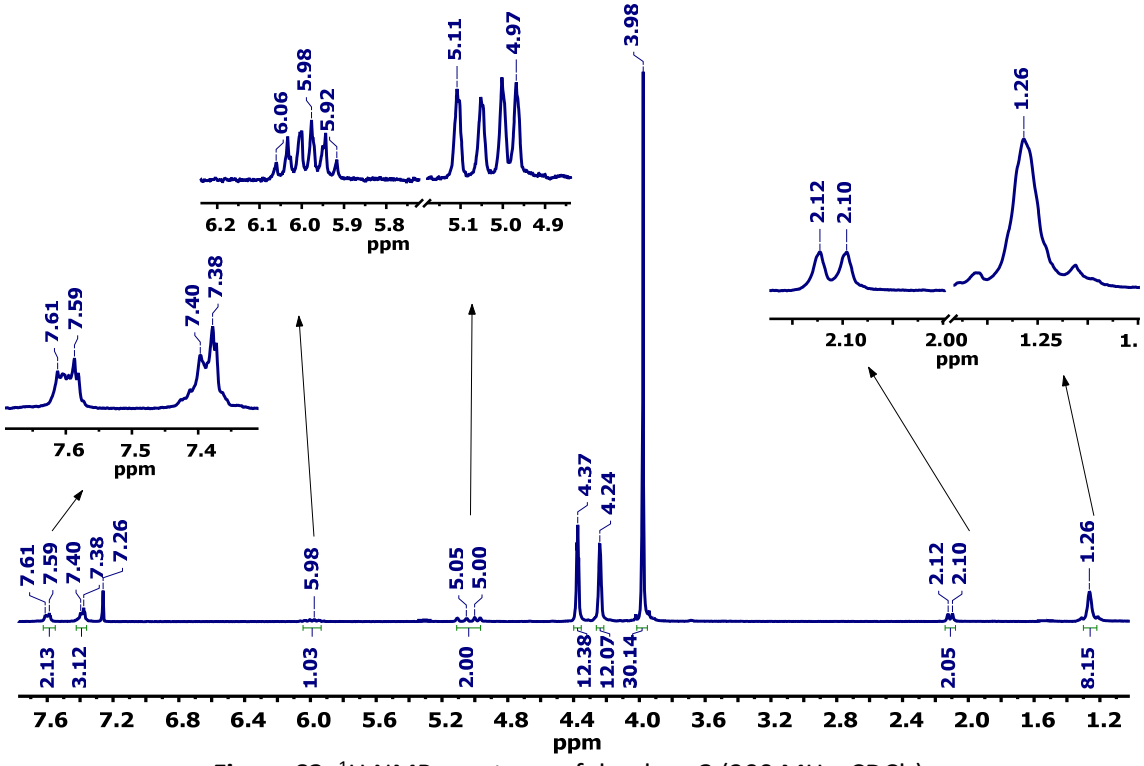

Figure S2: ^{1}H NMR spectrum of dendron **3** (300 MHz, $CDCl_3$).

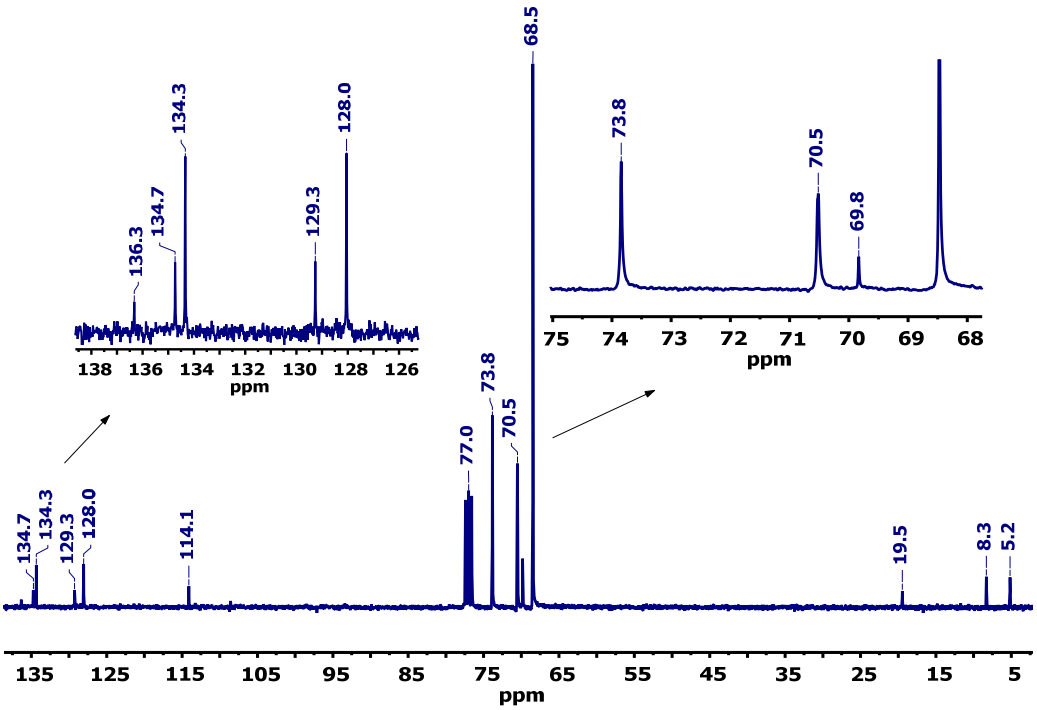

Figure S3: $^{13}C\{^{1}H\}$ NMR spectrum of dendron **3** (75 MHz, $CDCl_3$).

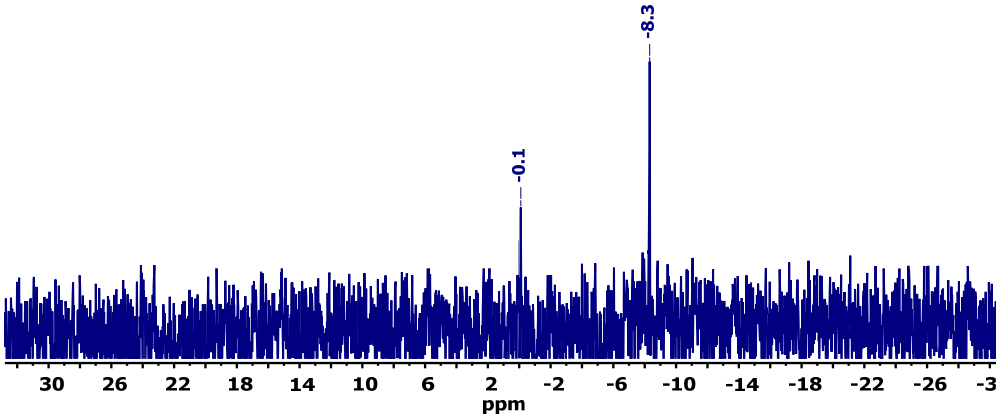

Figure S4: $^{29}Si\{^{1}H\}$ NMR spectrum of dendron **3** (59.6 MHz, $CDCl_3$).

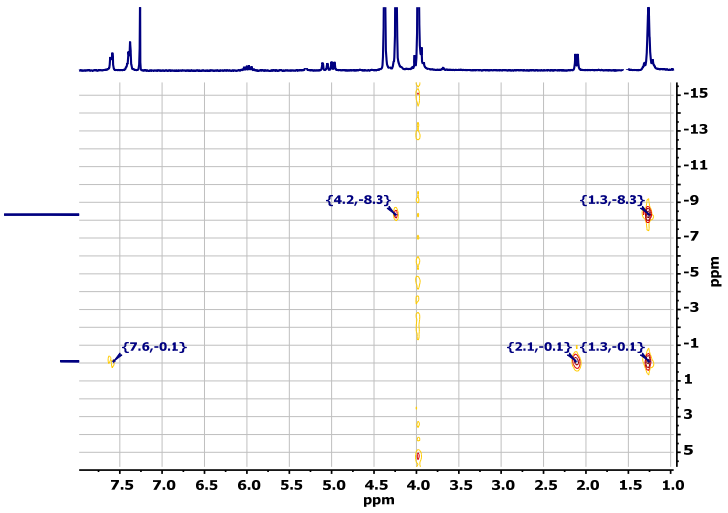

Figure S5: $\{^{1}H–^{29}Si\}$ HMBC spectrum of dendron **3** (300 MHz, 75 MHz, $CDCl_3$).

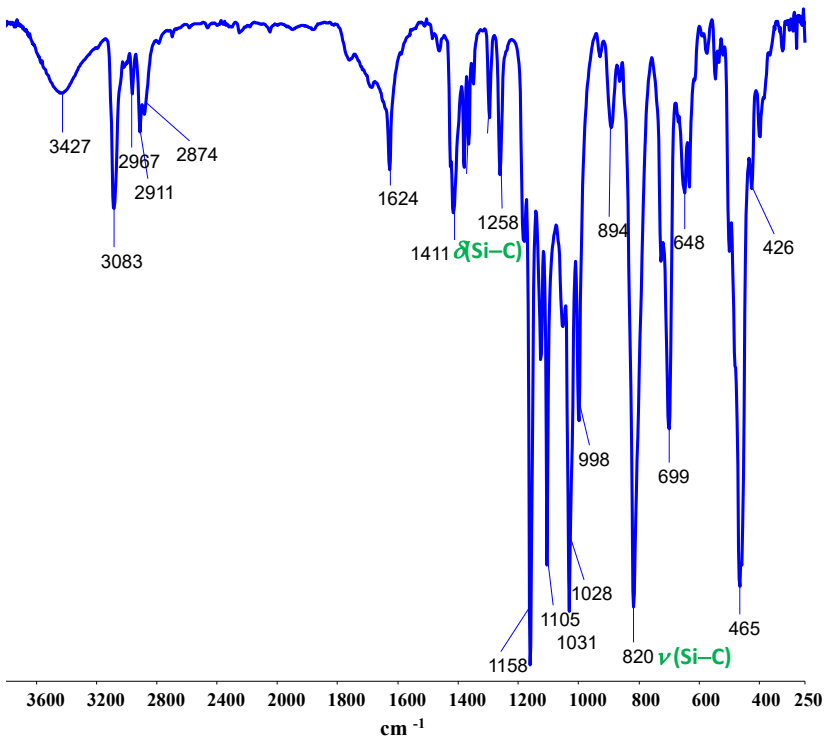

Figure S6: IR spectrum (KBr) of dendron **3.**

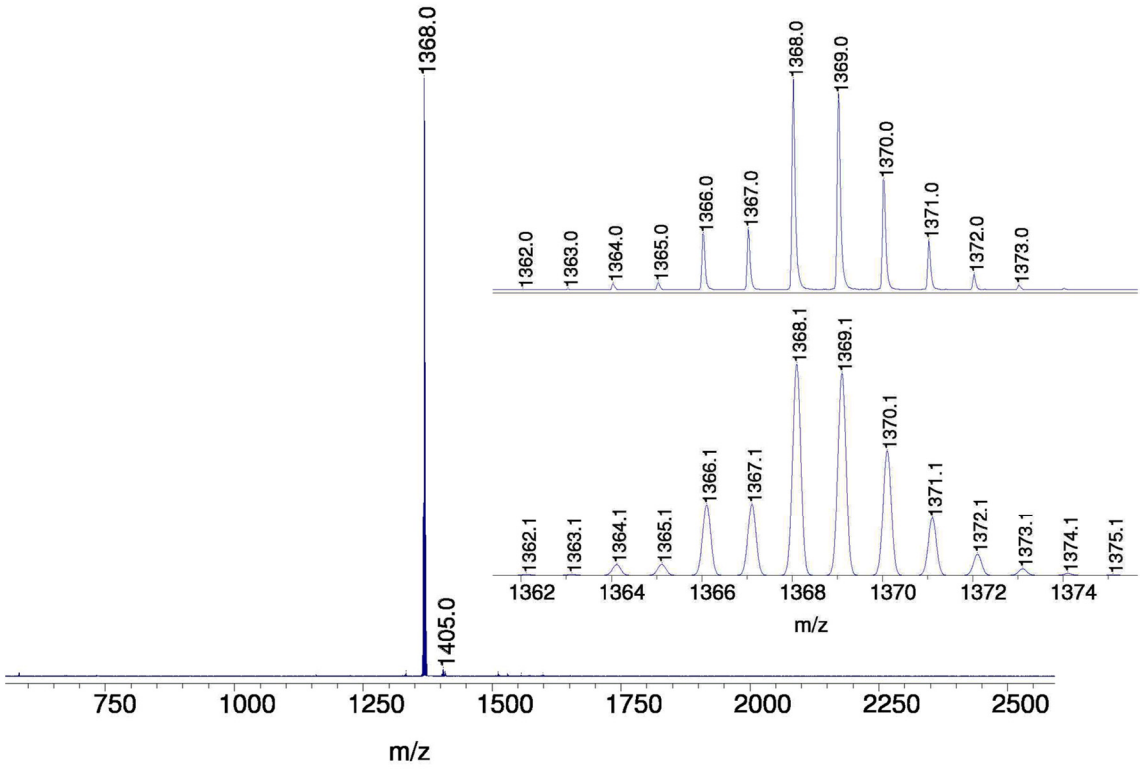

Figure S7: MALDI-TOF mass spectrometry of dendron **3**. Inset: isotopic distribution of the molecular ion peak (top: experimental; bottom: calculated).

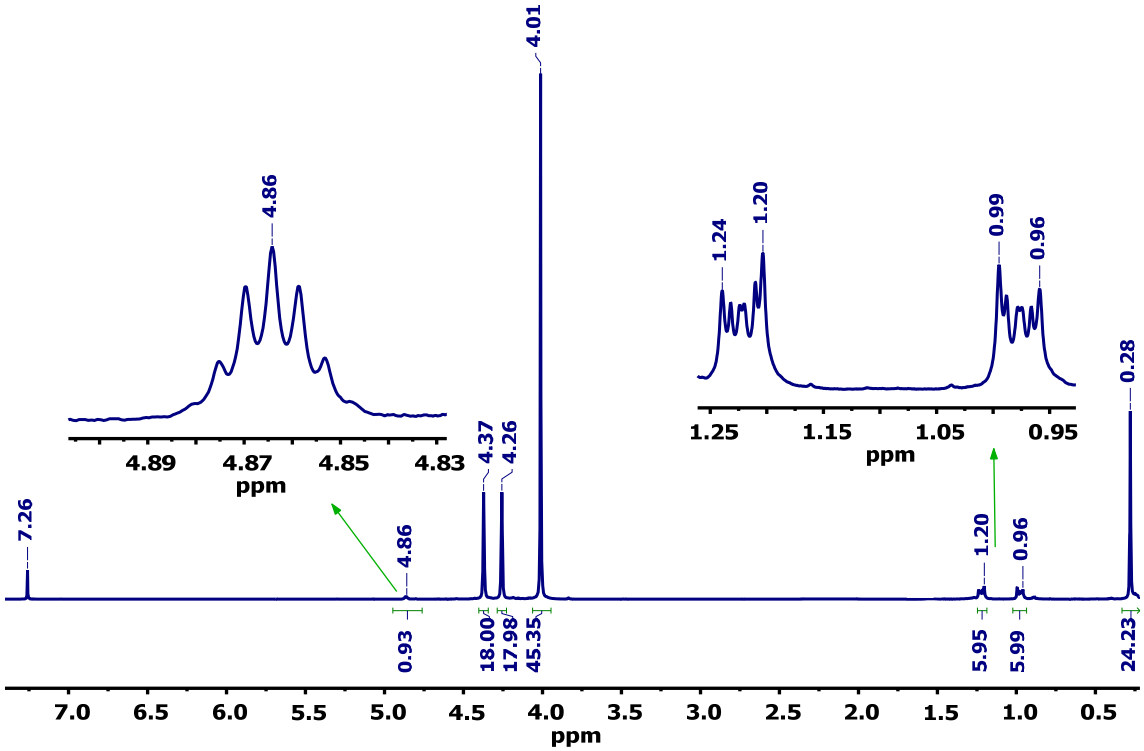

Figure S8: ^{1}H NMR spectrum of dendrimer **4** (500 MHz, $CDCl_3$).

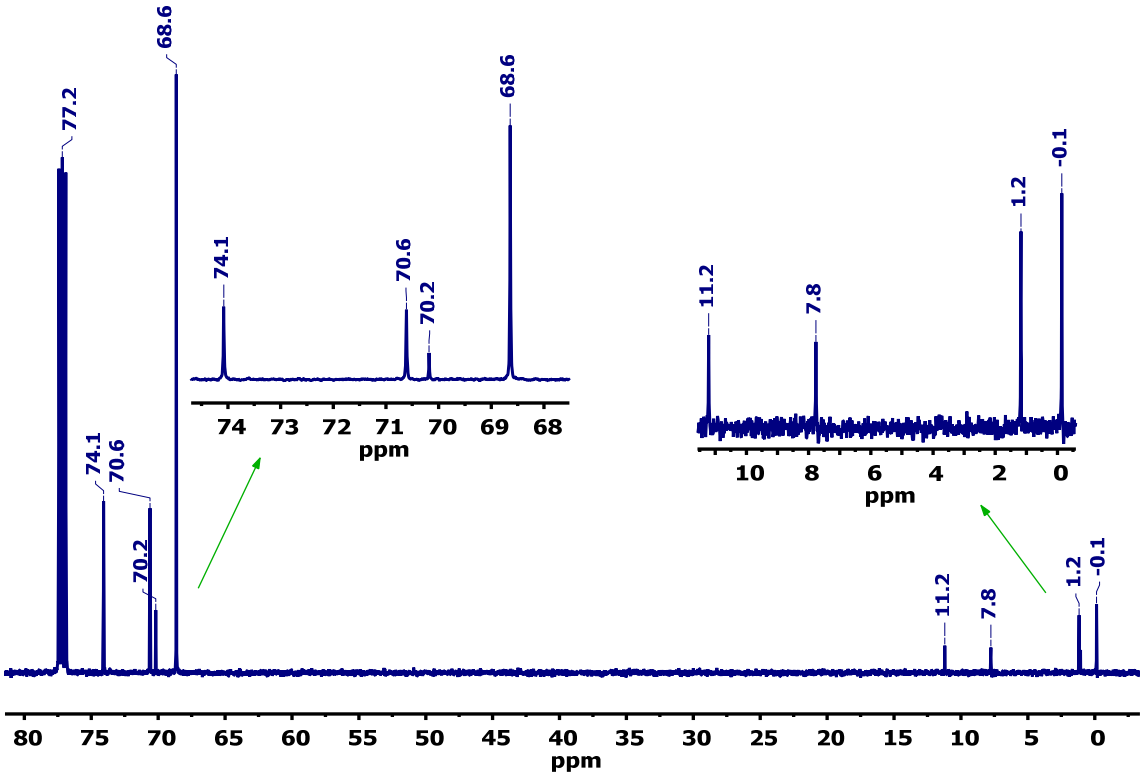

Figure S9: $^{13}C\{^{1}H\}$ NMR spectrum of dendrimer **4** (125 MHz, $CDCl_3$).

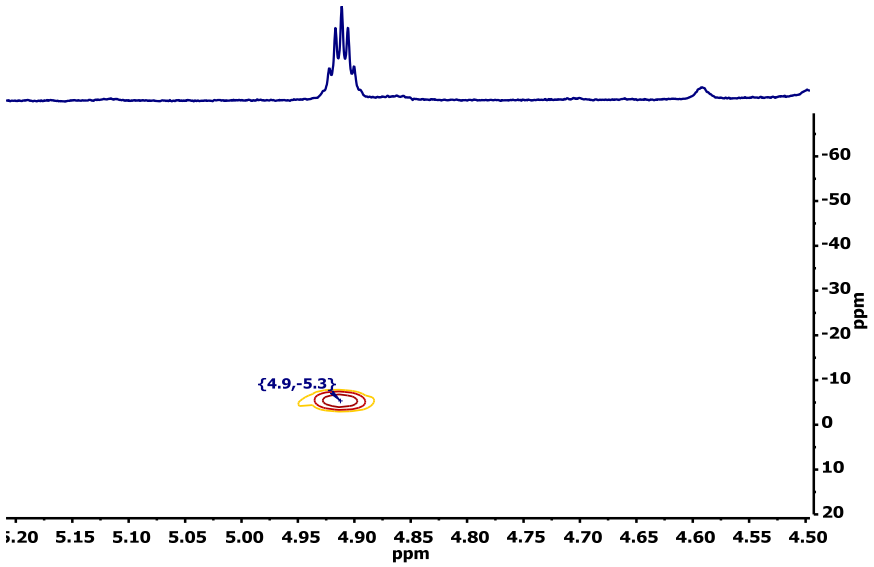

Figure S10: {^{1}H–^{29}Si} HMQC spectrum of dendrimer **4** (500 MHz, 99 MHz, $CDCl_3$).

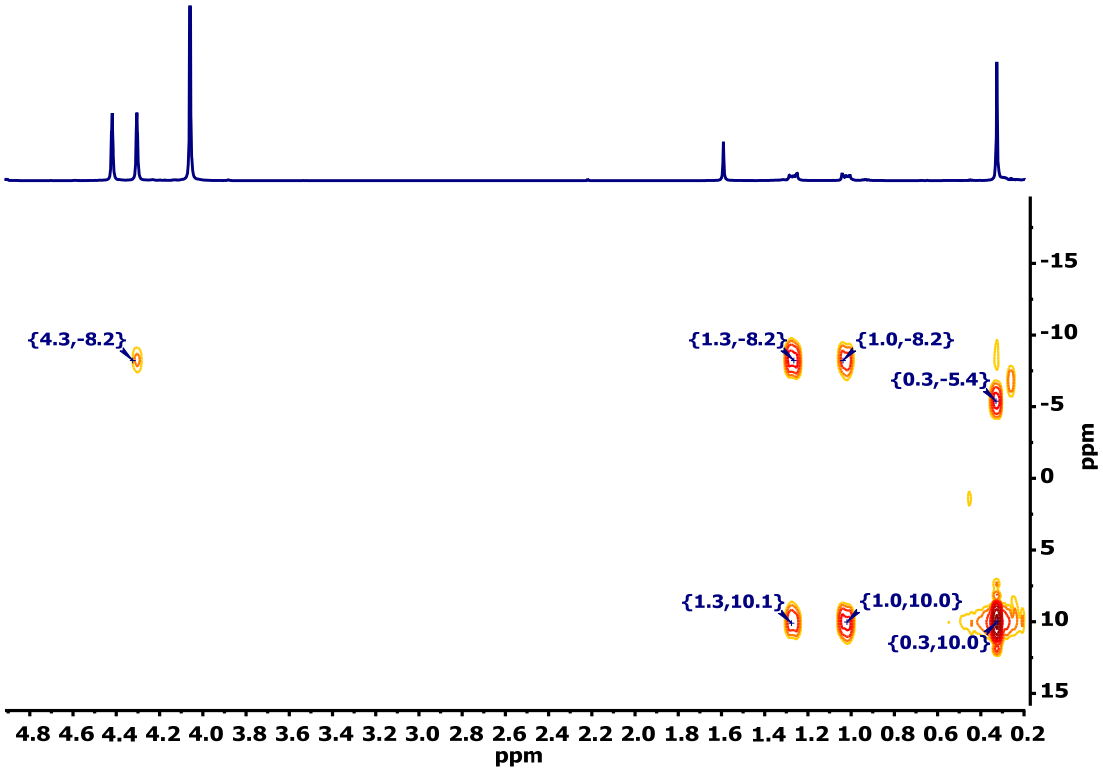

Figure S11: {^{1}H–^{29}Si} HMBC spectrum of dendrimer **4** (500 MHz, 99 MHz, $CDCl_3$).

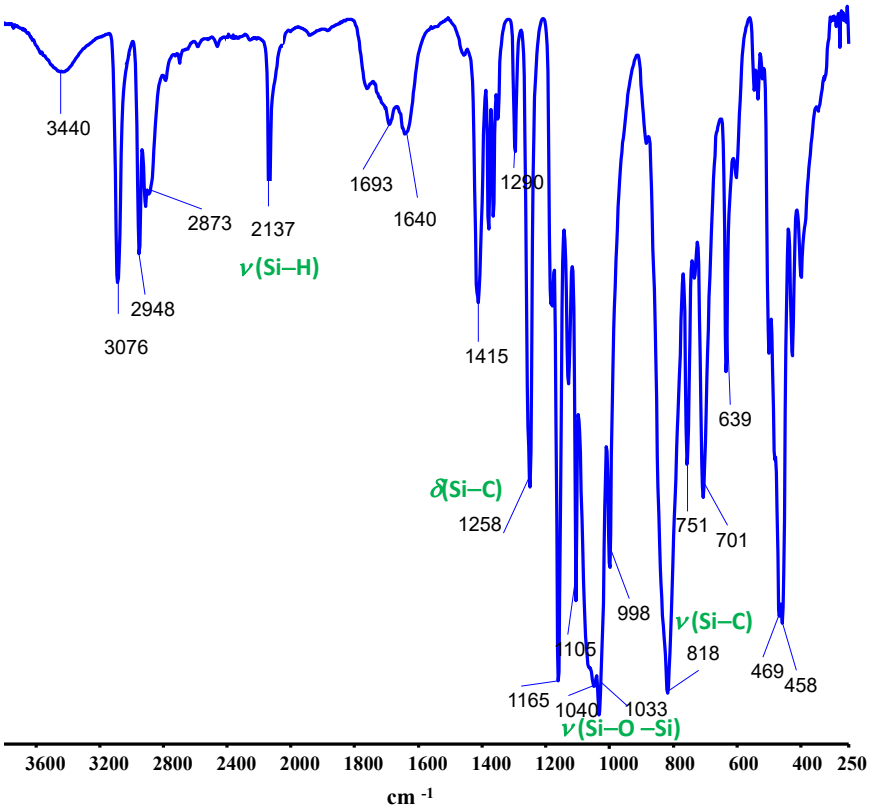

Figure S12: IR spectrum (KBr) of dendrimer **4.**

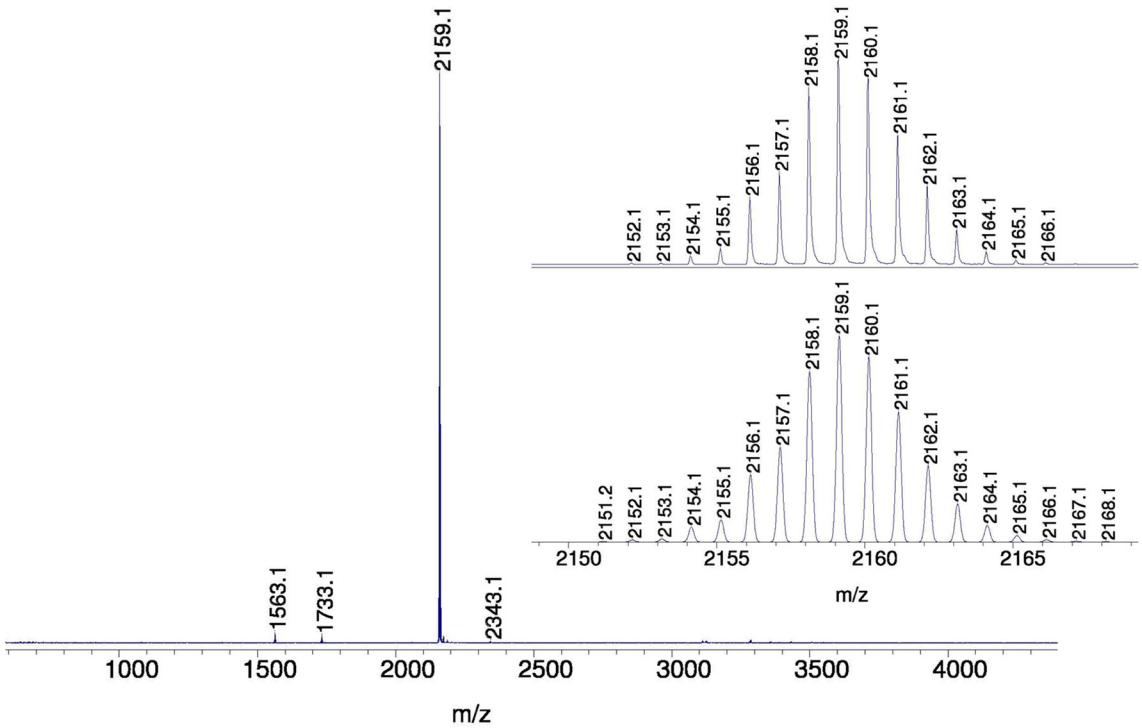

Figure S13: MALDI-TOF mass spectrometry of dendrimer **4**. Inset: isotopic distribution of the molecular ion peak (top: experimental; bottom: calculated).

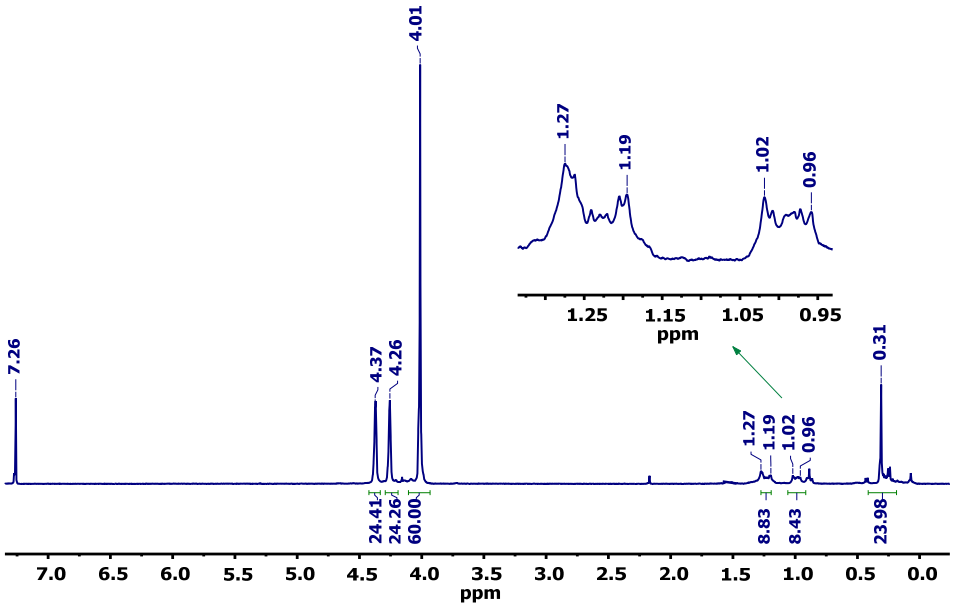

Figure S14: ^{1}H NMR spectrum of dendrimer **5** (300 MHz, $CDCl_3$).

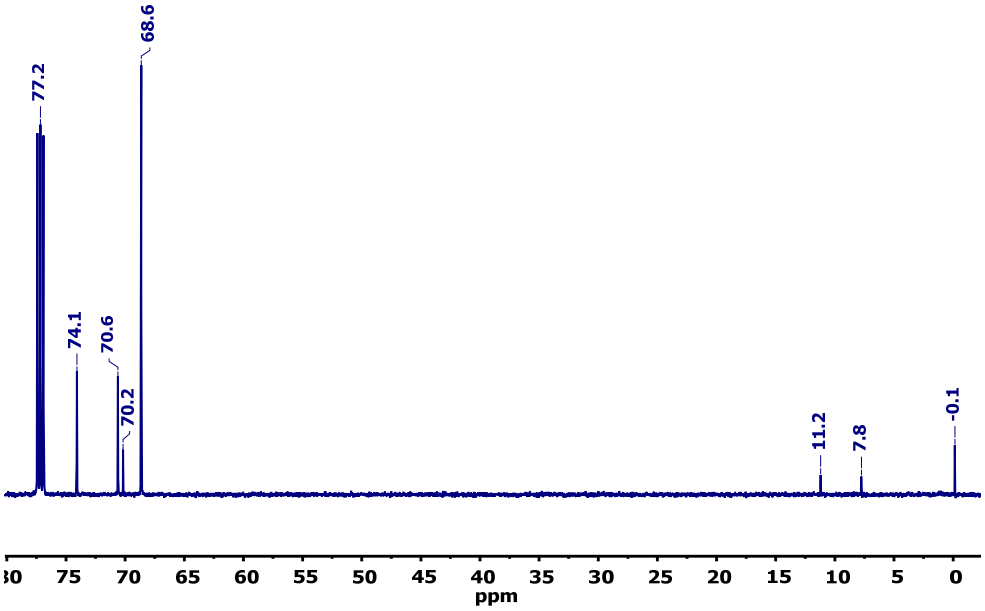

Figure S15: $^{13}C\{^{1}H\}$ NMR spectrum of dendrimer **5** (75 MHz, $CDCl_3$).

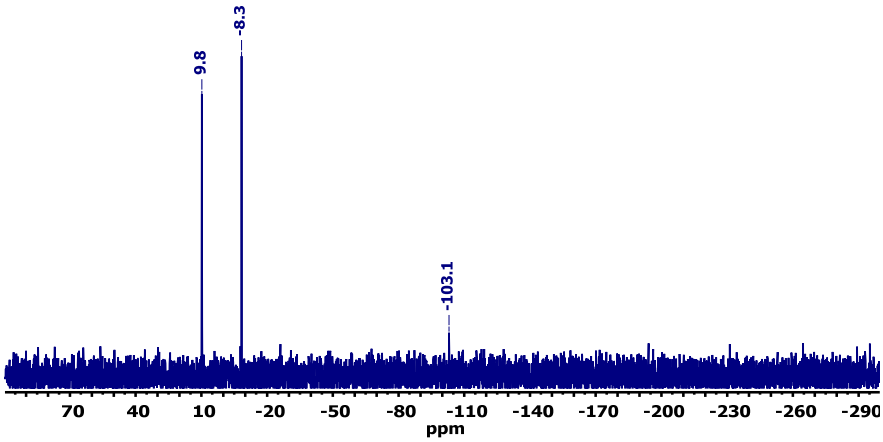

Figure S16: $^{29}Si\{^{1}H\}$ NMR spectrum of dendrimer **5** (59.6 MHz, $CDCl_3$).

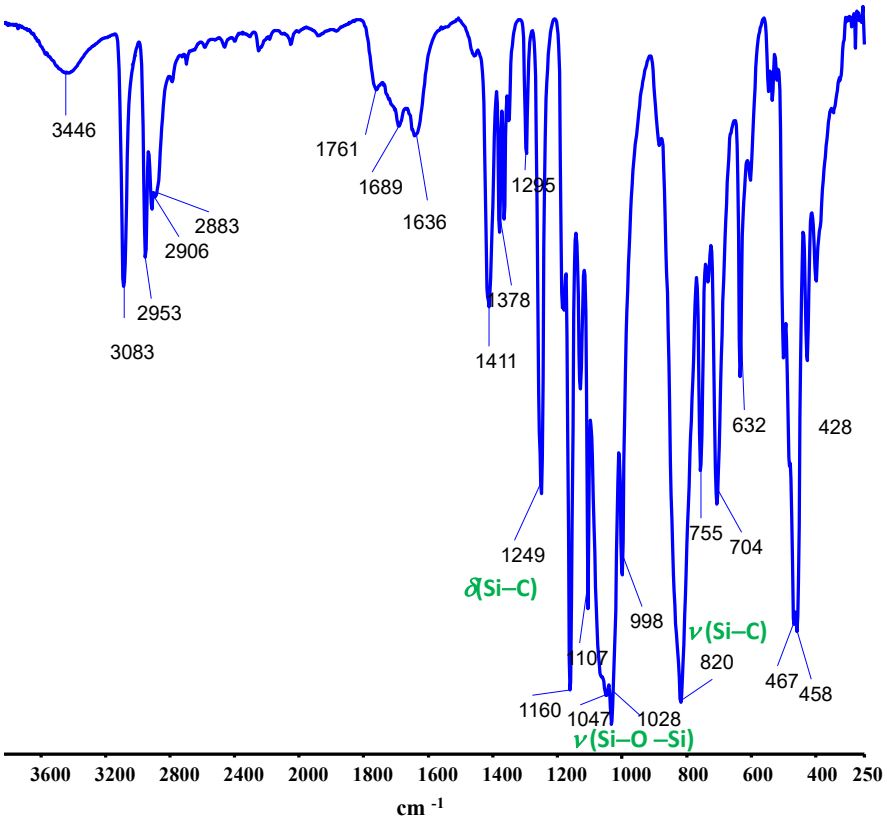

Figure S17: IR spectrum (KBr) of dendrimer **5.**

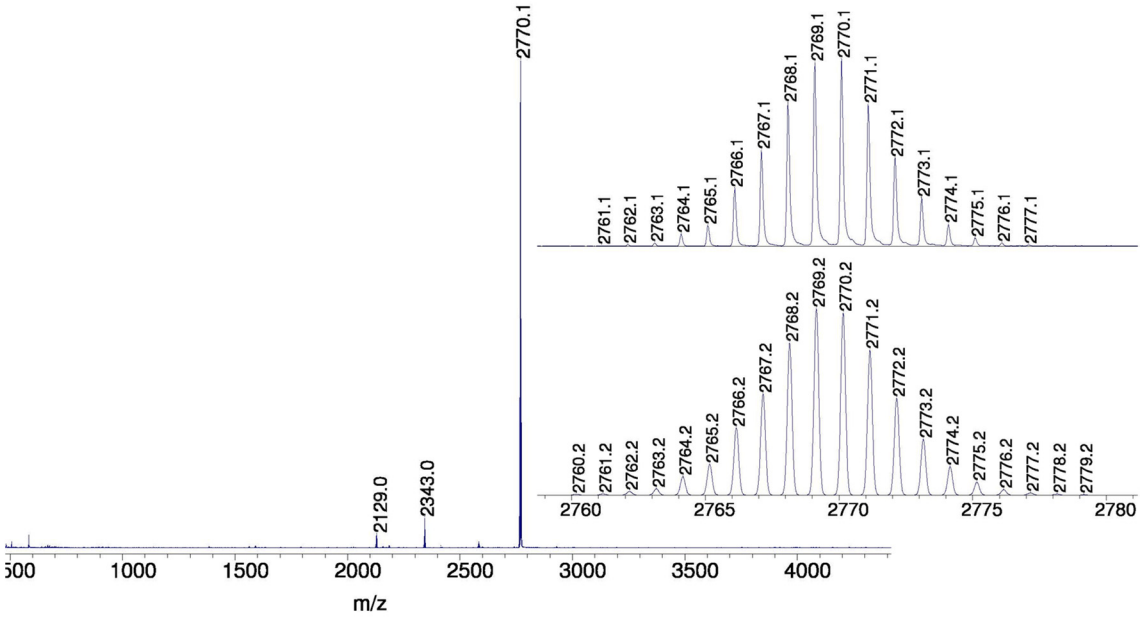

Figure S18: MALDI-TOF mass spectrometry of dendrimer **5**. Inset: isotopic distribution of the molecular ion peak (top: experimental; bottom: calculated).

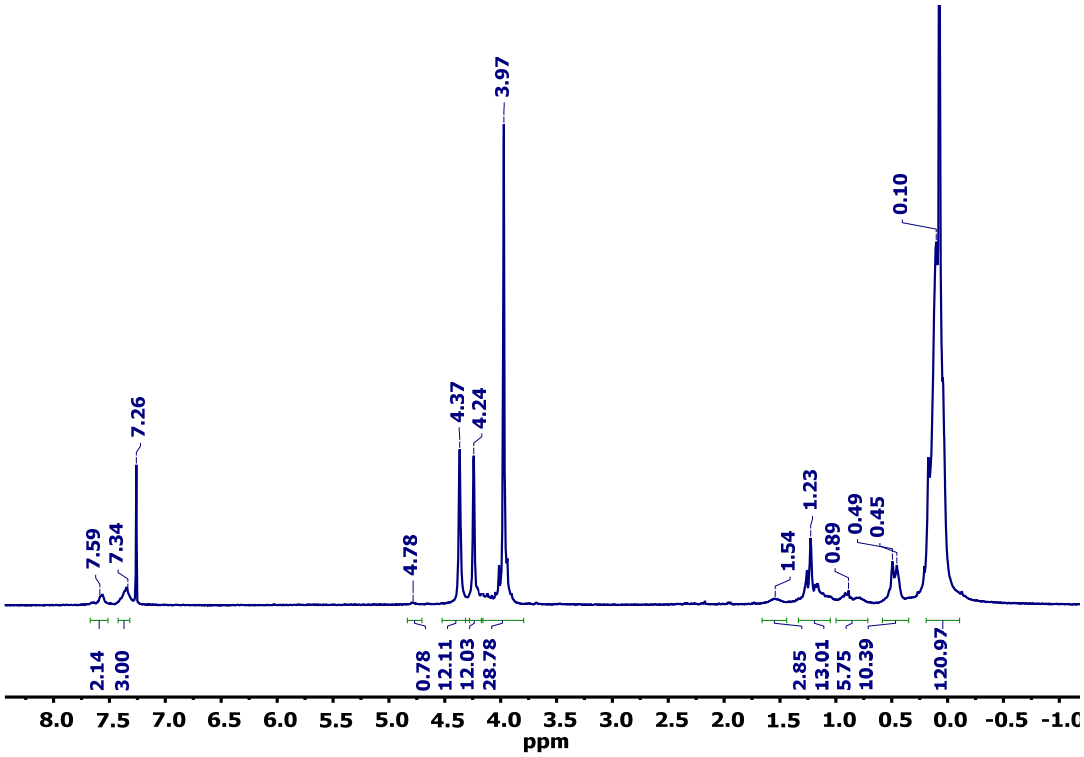

Figure S19: ^{1}H NMR spectrum of the reaction product resulting from the hydrosilylation of **3** and $Si[OSi(CH_3)_2H]_4$ (**I**): fraction obtained after the orange oil was dissolved in a small amount of CH_2Cl_2 and precipitated into *n*-hexane (300 MHz, $CDCl_3$).

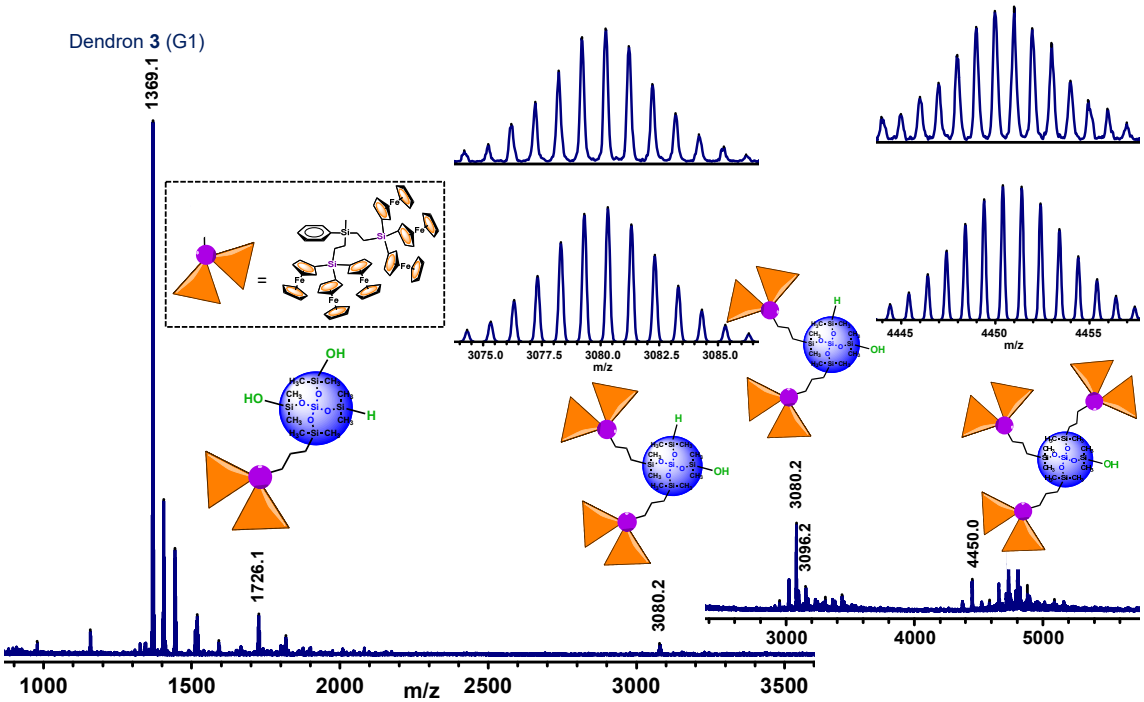

Figure S20. MALDI–TOF mass spectrum of the reaction product resulting from the hydrosilylation of **3** and $Si[OSi(CH_3)_2H]_4$ (**I**). The insets show the experimental and calculated isotopic patterns of peaks at *m/z* 3080.2 and 4450.0.

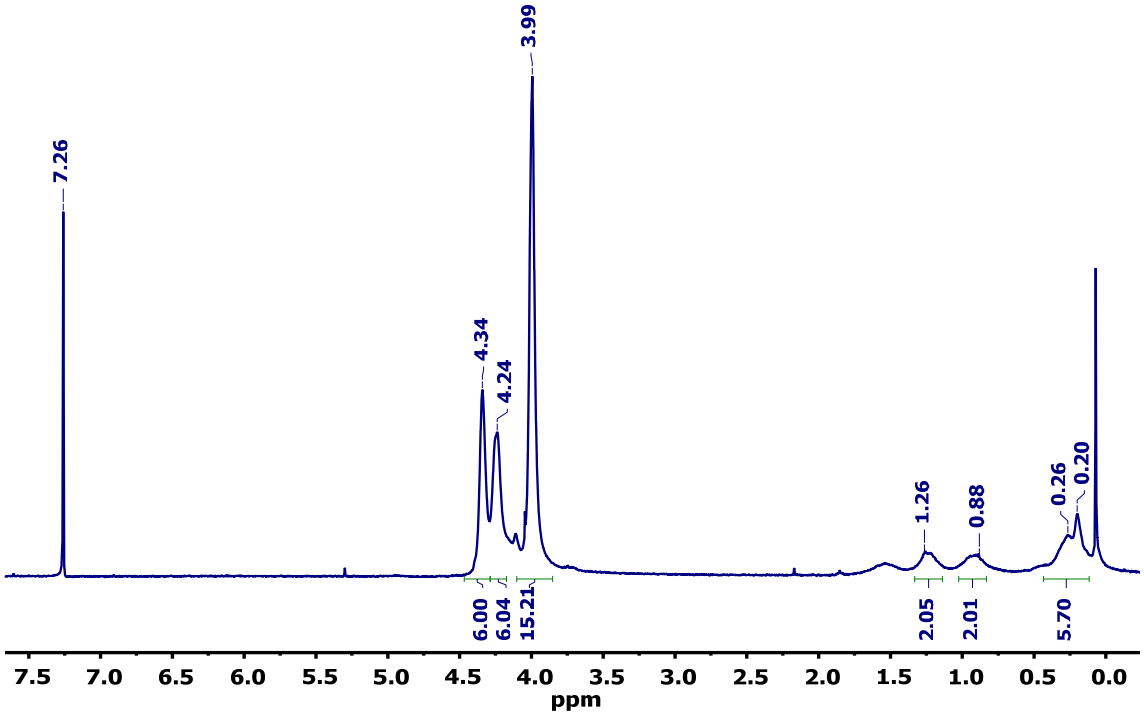

Figure S21: ^{1}H NMR spectrum of the reaction products $\mathbf{7_n}$–$\mathbf{9_n}$ from the hydrosilylation reaction of dendron **1** (**G0**) and poly(methylhidroxisilane) **II** (300 MHz, $CDCl_3$).

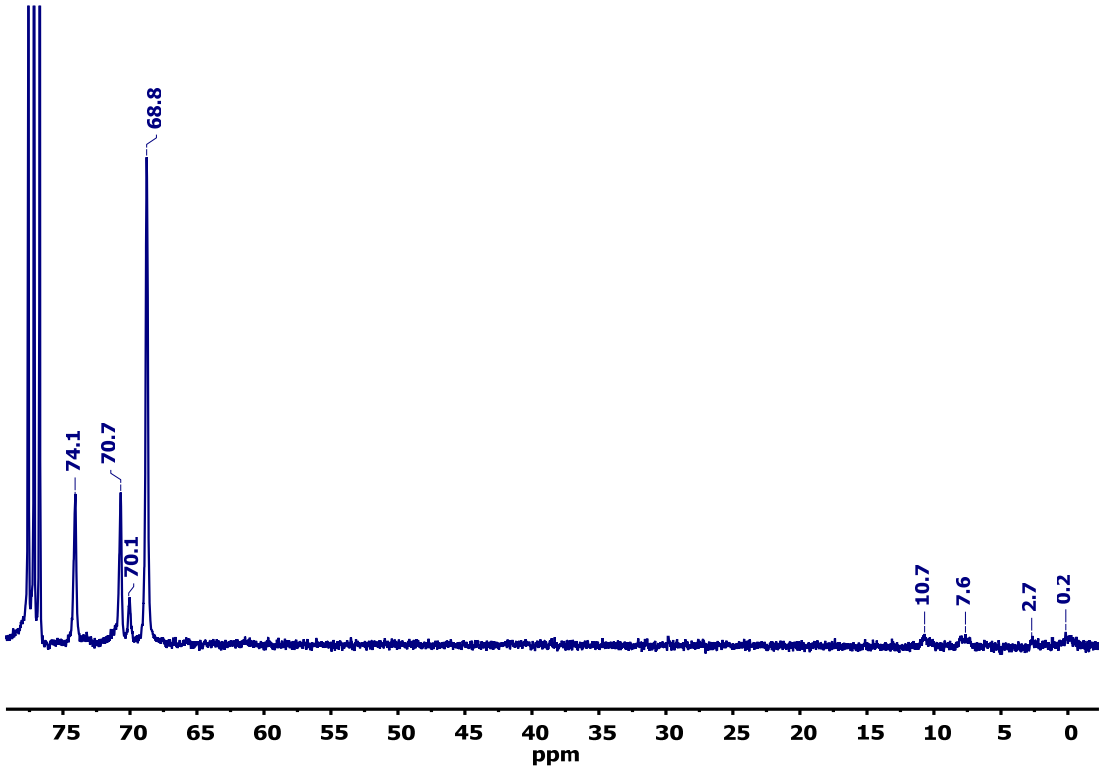

Figure S22: $^{13}C\{^{1}H\}$ NMR spectrum of the reaction products $\mathbf{7_n}$–$\mathbf{9_n}$ from the hydrosilylation reaction of dendron **1** (**G0**) and poly(methylhidroxisilane) **II** (75 MHz, $CDCl_3$).

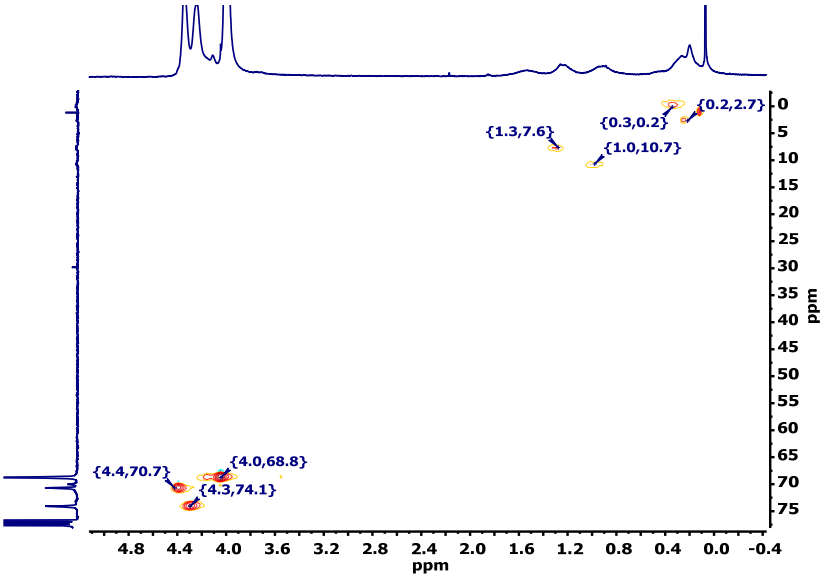

Figure S23: {^{1}H–^{13}C} HMQC spectrum of the reaction products **7$_n$–9$_n$** from the hydrosilylation reaction of dendron **1** (**G0**) and poly(methylhidroxisilane) **II** (500 MHz, 125 MHz, $CDCl_3$).

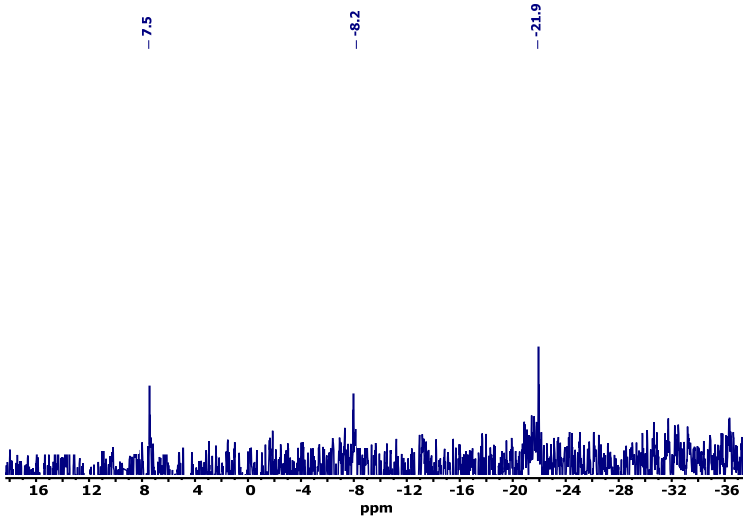

Figure S24: ^{29}Si{^{1}H} NMR spectrum of the reaction products **7$_n$–9$_n$** from the hydrosilylation reaction of dendron **1** (**G0**) and poly(methylhidroxisilane) **II** (59.6 MHz, $CDCl_3$).

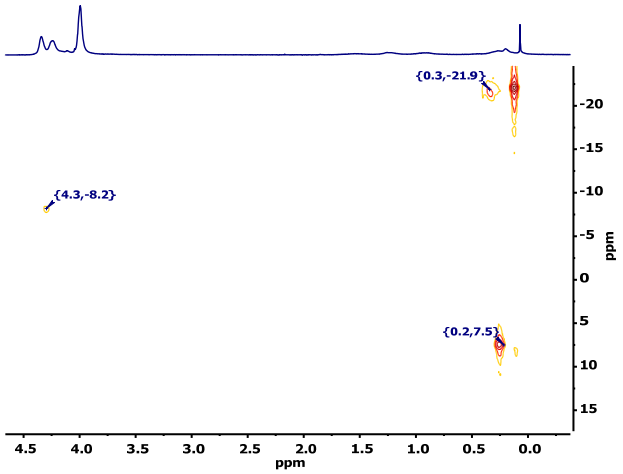

Figure S25: {^{1}H–^{29}Si} HMBC spectrum of the reaction products **7$_n$–9$_n$** from the hydrosilylation reaction of dendron **1** (**G0**) and poly(methylhidroxisilane) **II** (500 MHz, 99 MHz, $CDCl_3$).

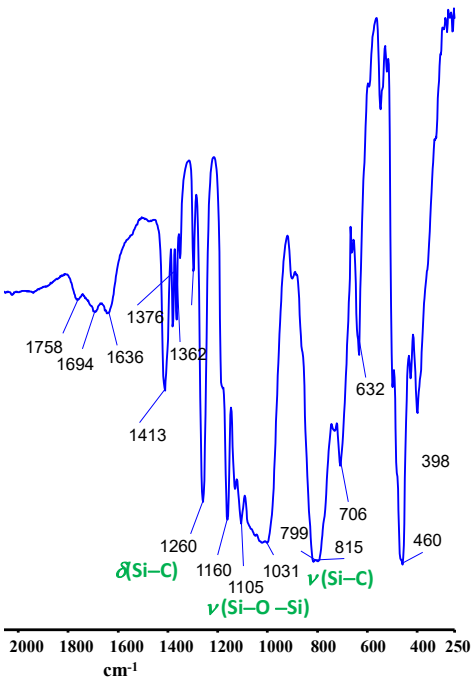

Figure S26: IR spectrum (KBr) of the reaction products $\mathbf{7_n}$–$\mathbf{9_n}$ from the hydrosilylation reaction of dendron **1** (**G0**) and poly(methylhidroxisilane) **II.**

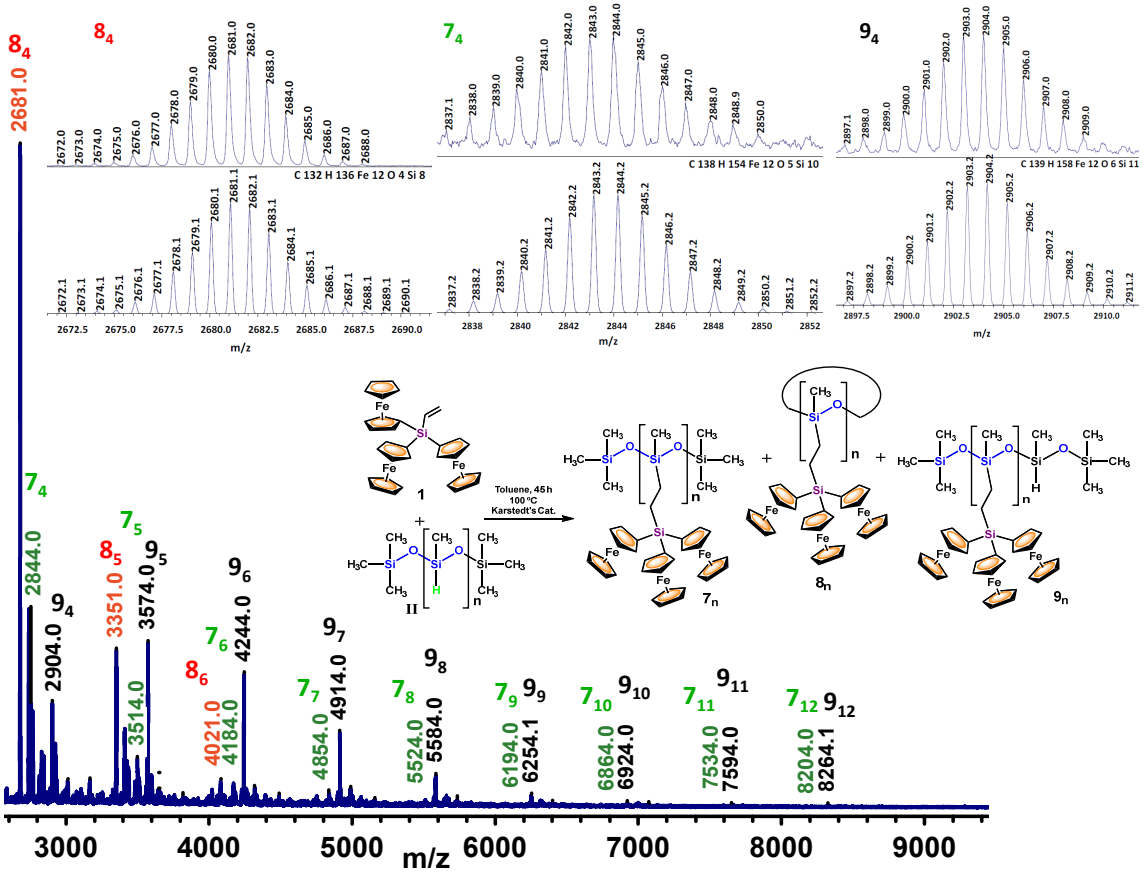

Figure S27: MALDI-TOF of $\mathbf{7_n}$–$\mathbf{9_n}$ from the hydrosilylation reaction of dendron **1** (**G0**) and poly(methylhidroxisilane) **II**. The insets show the experimental and calculated isotopic patterns of the peaks at m/z 2681.0, 2844.0 and 2904.0.

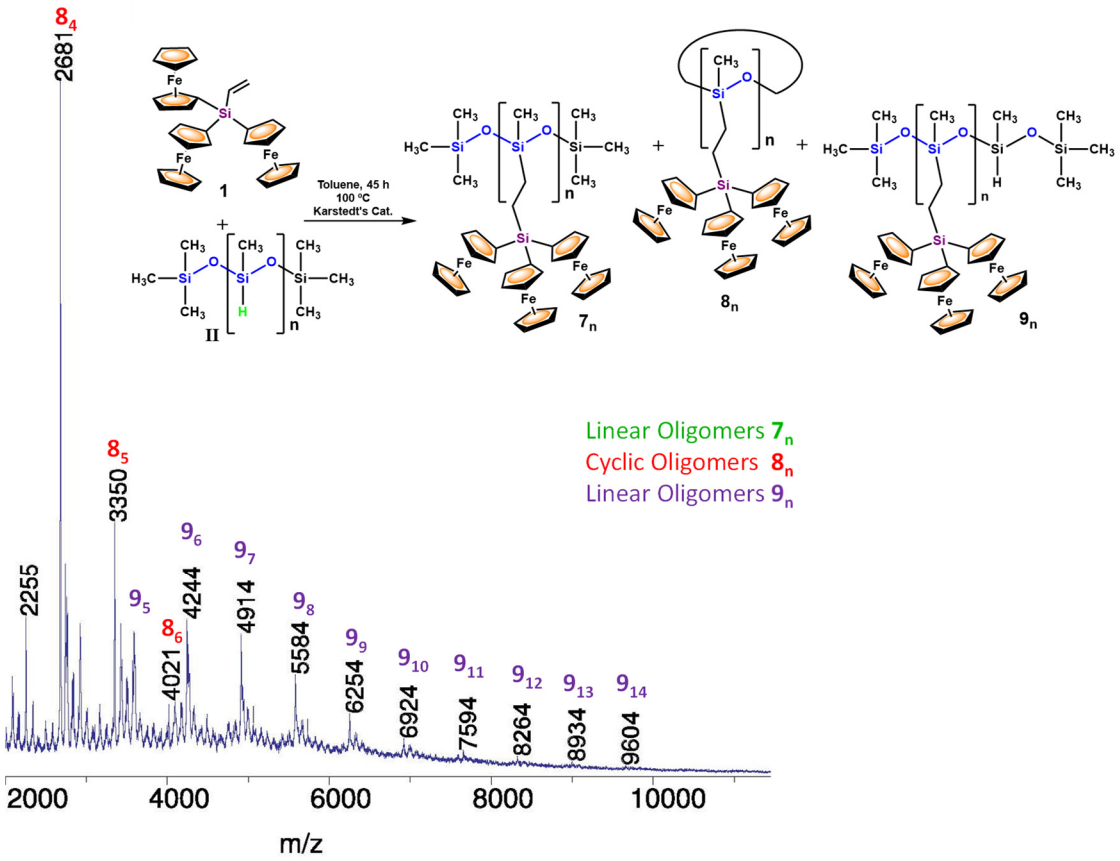

Figure S28: MALDI-TOF mass spectrometry of the reaction products $\mathbf{7_n}$–$\mathbf{9_n}$ from the hydrosilylation reaction of dendron **1** (**G0**) and poly(methylhidroxisilane) **II** after the first precipitate was dissolved again in a small amount of CH_2Cl_2 and precipitated into methanol. *m/z* 2000 deflection.

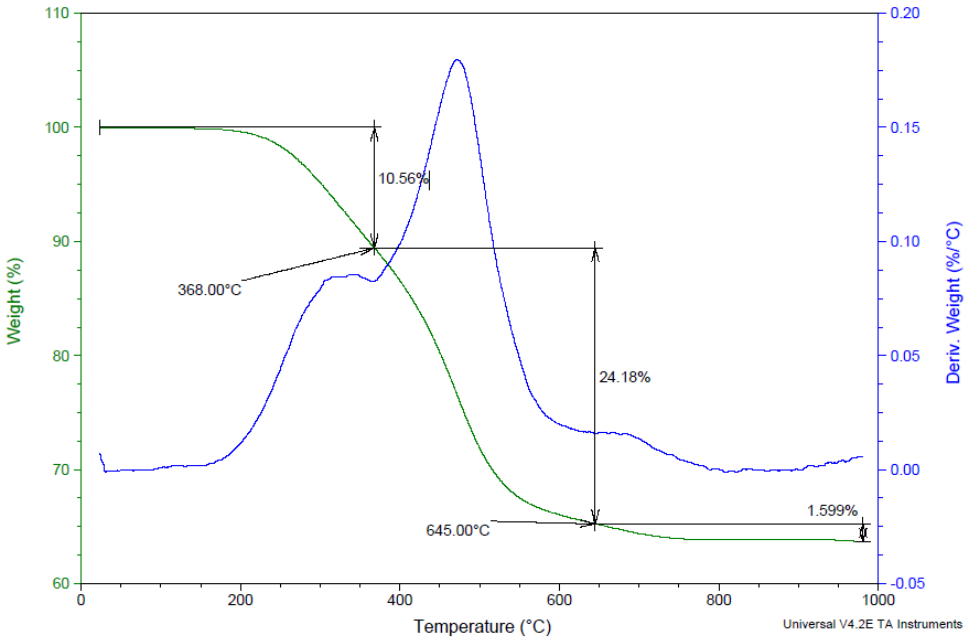

Figure S29. TGA thermograms of the mixture of dendronized polymers $\mathbf{7_n}$–$\mathbf{9_n}$ under N_2 at a heating rate of 10 °C min^{-1}.

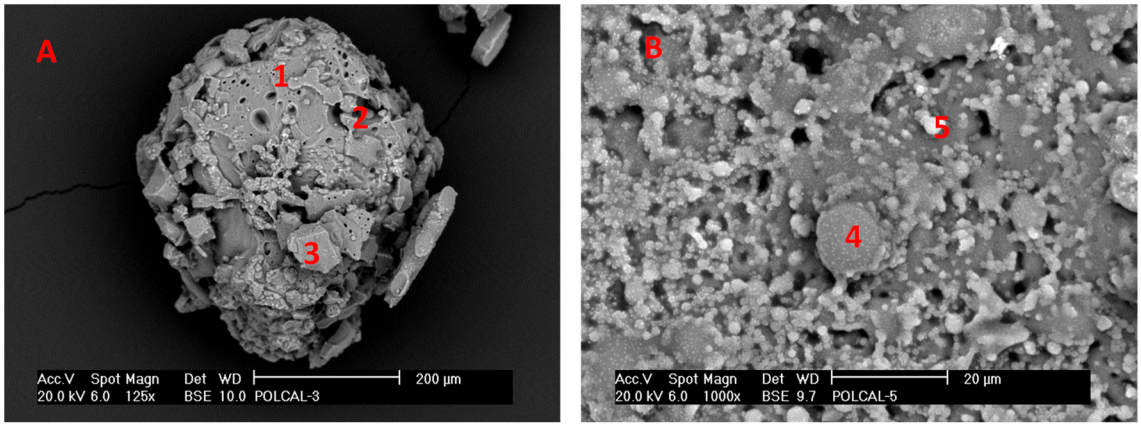

Figure S30. SEM images of the ceramic material obtained by the pyrolysis of the mixture of dendronized polymers $\mathbf{7}_n$–$\mathbf{9}_n$, under nitrogen atmosphere.

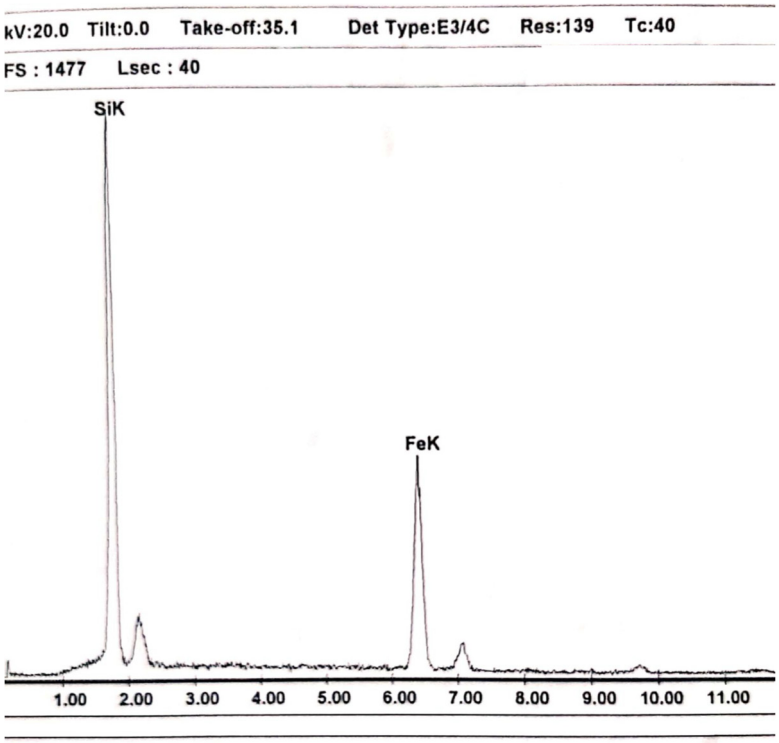

EDAX ZAF Quantification (Standardless)
Element Normalized
SEC Table : Default

Element	Wt %	At %	K-Ratio	Z	A	F
SiK	50.17	66.69	0.3278	1.0520	0.6205	1.0008
FeK	49.83	33.31	0.4613	0.9366	0.9885	1.0000
Total	100.00	100.00				

Figure S31. EDX analyses of the ceramic residue obtained by the pyrolysis of $\mathbf{7}_n$–$\mathbf{9}_n$ (at 1000°C under nitrogen atmosphere), point 1 in Figure S30A.

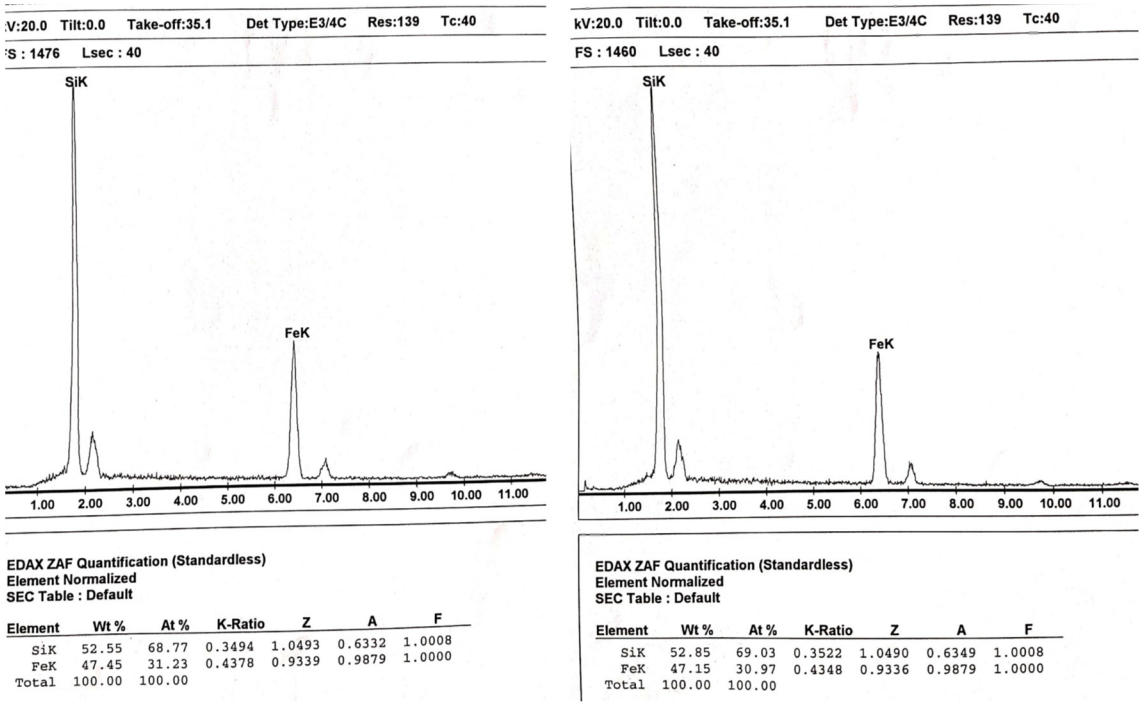

Figure S32. EDX analyses of the ceramic residue obtained by the pyrolysis of **7**$_n$–**9**$_n$ (at 1000°C under nitrogen atmosphere), points 2 (left) and 3 (right) of the Figure S30A.

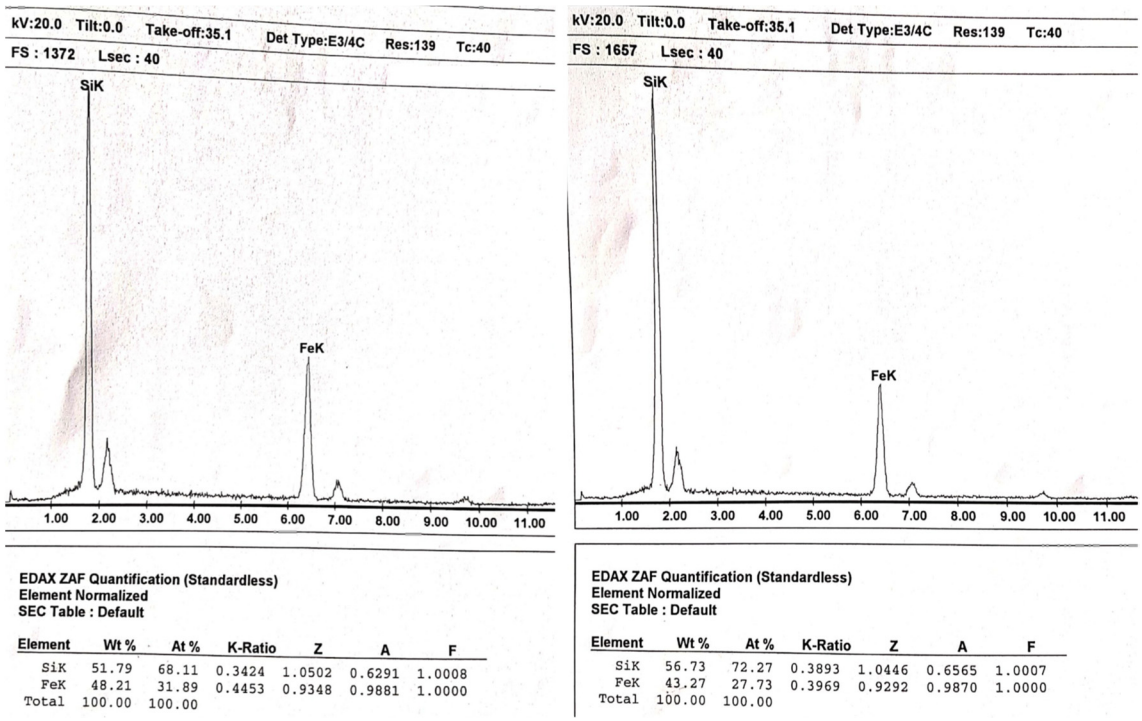

Figure S33. EDX analyses of the ceramic residue obtained by the pyrolysis of **7**$_n$–**9**$_n$ (at 1000°C under nitrogen atmosphere), points 4 (left) and 5 (right) of the Figure S30B.

3. X-Ray Structures of Dendron 3 (CCDC 2105207) and Dendrimer 4 (CCDC 2105208)

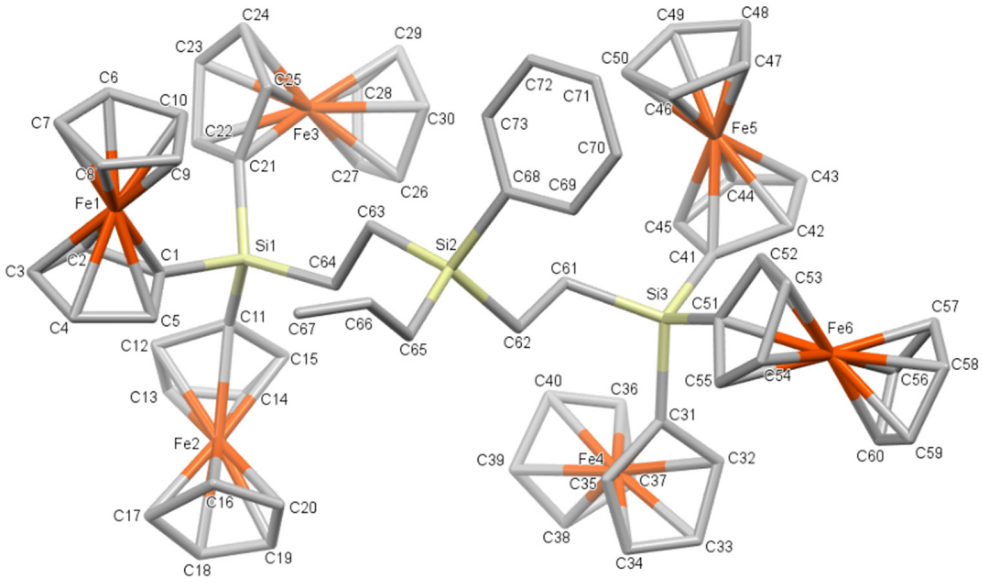

Figure S34. Asymmetric unit of Dendron **3** with atoms labelled. Hydrogen atoms have been omitted for clarity.

Table S1. Sample and crystal data for 3.

CCDC code	2105207	
Chemical formula	$C_{73}H_{72}Fe_6Si_3$	
Formula weight	1368.67 g/mol	
Temperature	296(2) K	
Wavelength	0.71073 Å	
Crystal size	0.080 x 0.140 x 0.250 mm	
Crystal habit	clear intense orange prismatic	
Crystal system	monoclinic	
Space group	$P2_1/n$	
Unit cell dimensions	a = 20.1982(4) Å	α = 90°
	b = 12.5410(2) Å	β = 95.546(1)°
	c = 24.6180(5) Å	γ = 90°
Volume	6206.7(2) Å^3	
Z	4	
Density (calculated)	1.465 g/cm^3	
Absorption coefficient	1.466 mm^{-1}	
F(000)	2832	

Table S2. Data collection and structure refinement for 3.

Theta range for data collection	1.37 to 25.40°	
Index ranges	-24<=h<=22, -15<=k<=15, -29<=l<=29	
Reflections collected	53353	
Independent reflections	11423 [R(int) = 0.0627]	
Structure solution technique	direct methods	
Structure solution program	SHELXS-97 (Sheldrick, 2008)	
Refinement method	Full-matrix least-squares on F^2	
Refinement program	SHELXL-2018/3 (Sheldrick, 2018)	
Function minimized	$\Sigma\, w(F_o^2 - F_c^2)^2$	
Data / restraints / parameters	11423 / 5 / 730	
Goodness-of-fit on F^2	1.022	
Final R indices	7071 data; I>2σ(I)	$R_1 = 0.0620$, $wR_2 = 0.1540$
	all data	$R_1 = 0.1128$, $wR_2 = 0.1851$
Weighting scheme	$w=1/[\sigma^2(F_o^2)+(0.0826P)^2+12.7017P$ where $P=(F_o^2+2F_c^2)/3$	
Largest diff. peak and hole	2.533 and -1.612 eÅ^{-3}	
R.M.S. deviation from mean	0.091 eÅ^{-3}	

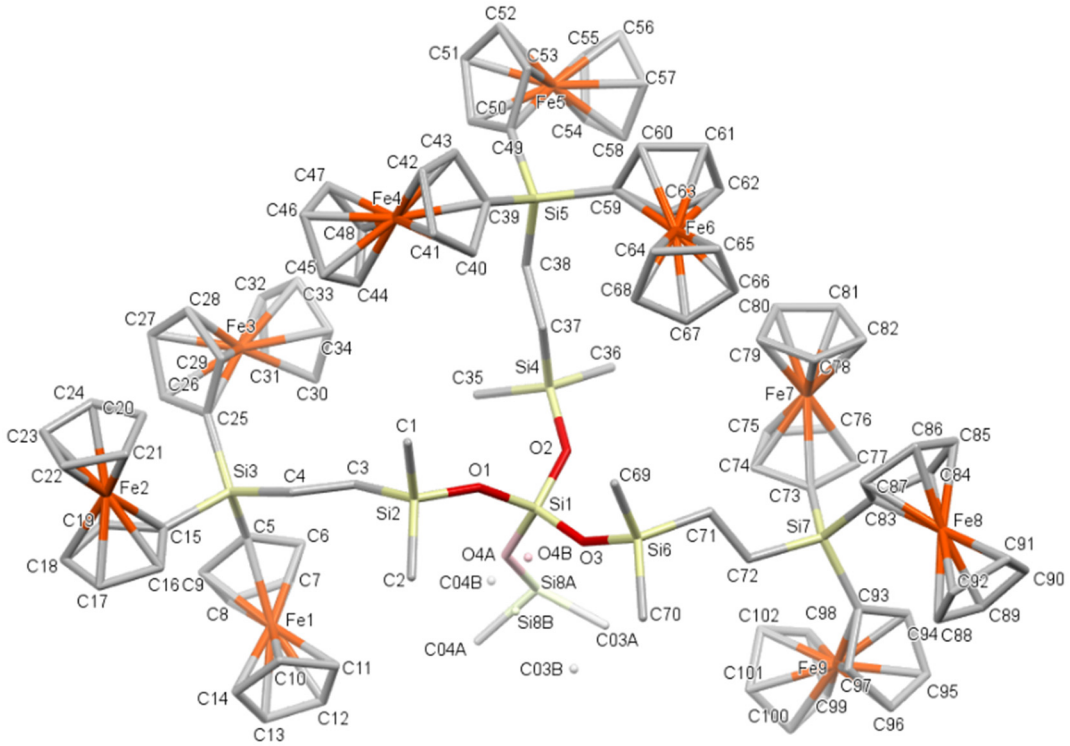

Figure S35. Asymmetric unit of Dendrimer **4** with atoms labelled. Hydrogen atoms have been omitted for clarity. Atoms O4, Si8, C03 and C04 (depicted in lighter shades) are disordered in two positions A and B with 60% and 40% occupation respectively.

Table S3. Sample and crystal data for 4.

CCDC code	2105208	
Chemical formula	$C_{104}H_{118}Fe_9O_4Si_8$	
Formula weight	2159.35 g/mol	
Temperature	296(2) K	
Wavelength	0.71073 Å	
Crystal size	0.010 x 0.040 x 0.220 mm	
Crystal habit	clear light orange needle	
Crystal system	monoclinic	
Space group	$P2_1/n$	
Unit cell dimensions	a = 30.048(1) Å	α = 90°
	b = 9.2412(2) Å	β = 91.762(1)°
	c = 35.879(1) Å	γ = 90°
Volume	9958.2(5) $Å^3$	
Z	4	
Density (calculated)	1.440 g/cm^3	
Absorption coefficient	1.418 mm^{-1}	
F(000)	4480	

Table S4. Data collection and structure refinement for 4.

Theta range for data collection	1.85 to 25.38°	
Index ranges	-34<=h<=36, -11<=k<=11, -43<=l<=43	
Reflections collected	101581	
Independent reflections	18227 [R(int) = 0.1550]	
Max. and min. transmission	0.9860 and 0.7460	
Refinement method	Full-matrix least-squares on F^2	
Refinement program	SHELXL-2018/3 (Sheldrick, 2018)	
Function minimized	$\Sigma\, w(F_o^2 - F_c^2)^2$	
Data / restraints / parameters	18227 / 19 / 1116	
Goodness-of-fit on F^2	1.042	
Final R indices	7657 data; I>2σ(I)	R_1 = 0.0750, wR_2 = 0.1450
	all data	R_1 = 0.2087, wR_2 = 0.1888
Weighting scheme	$w=1/[\sigma^2(F_o^2)+(0.0728P)^2+3.2181P]$ where $P=(F_o^2+2F_c^2)/3$	
Largest diff. peak and hole	1.143 and -1.148 $eÅ^{-3}$	
R.M.S. deviation from mean	0.092 $eÅ^{-3}$	

Table S5. Distances between iron atoms in molecules 3 and 4 (shortest values in *italics* and largest ones in **bold**).

Distances between metal centers bonded to the same silicon atom (Å)		
3	Fe1-Fe2	6.117(1)
	Fe1-Fe3	6.093(1)
	Fe2-Fe3	6.026(1)
	Fe4-Fe5	**6.164(1)**
	Fe4-Fe6	6.040(1)
	Fe5-Fe6	*5.401(1)*
4	Fe1-Fe2	6.061(2)
	Fe1-Fe3	**6.160(2)**
	Fe2-Fe3	5.898(2)
	Fe4-Fe5	6.099(1)
	Fe4-Fe6	6.201(2)
	Fe5-Fe6	5.932(2)
	Fe7-Fe8	*5.806(2)*
	Fe7-Fe9	6.028(2)
	Fe8-Fe9	5.896(2)
Distances between metal centers bonded to a different silicon atom (Å)		
3	Fe1-Fe4	10.784(1)
	Fe1-Fe5	11.063(1)
	Fe1-Fe6	**12.730(1)**
	Fe2-Fe4	*6.967(1)*
	Fe2-Fe5	10.201(1)
	Fe2-Fe6	11.559(1)
	Fe3-Fe4	8.312(2)
	Fe3-Fe5	7.261(1)
	Fe3-Fe6	11.111(1)
4	Fe1-Fe4	10.409(2)
	Fe1-Fe5	13.456(2)
	Fe1-Fe6	13.310(2)
	Fe1-Fe7	12.894(2)
	Fe1-Fe8	15.623(2)
	Fe1-Fe9	12.512(2)
	Fe2-Fe4	8.840(2)
	Fe2-Fe5	13.809(2)
	Fe2-Fe6	13.875(2)
	Fe2-Fe7	15.998(2)
	Fe2-Fe8	**18.497(2)**
	Fe2-Fe9	17.024(2)
	Fe3-Fe4	6.388(2)
	Fe3-Fe5	9.042(2)
	Fe3-Fe6	11.023(2)
	Fe3-Fe7	12.577(2)
	Fe3-Fe8	16.656(2)
	Fe3-Fe9	14.912(2)
	Fe4-Fe7	10.671(2)
	Fe4-Fe8	13.909(2)
	Fe4-Fe9	14.586(2)
	Fe5-Fe7	8.827(2)
	Fe5-Fe8	13.651(2)
	Fe5-Fe9	14.244(2)
	Fe6-Fe7	*6.224(2)*
	Fe6-Fe8	8.857(2)
	Fe6-Fe9	11.248(2)

4. Electrochemistry of dendritic compounds 1-9$_n$

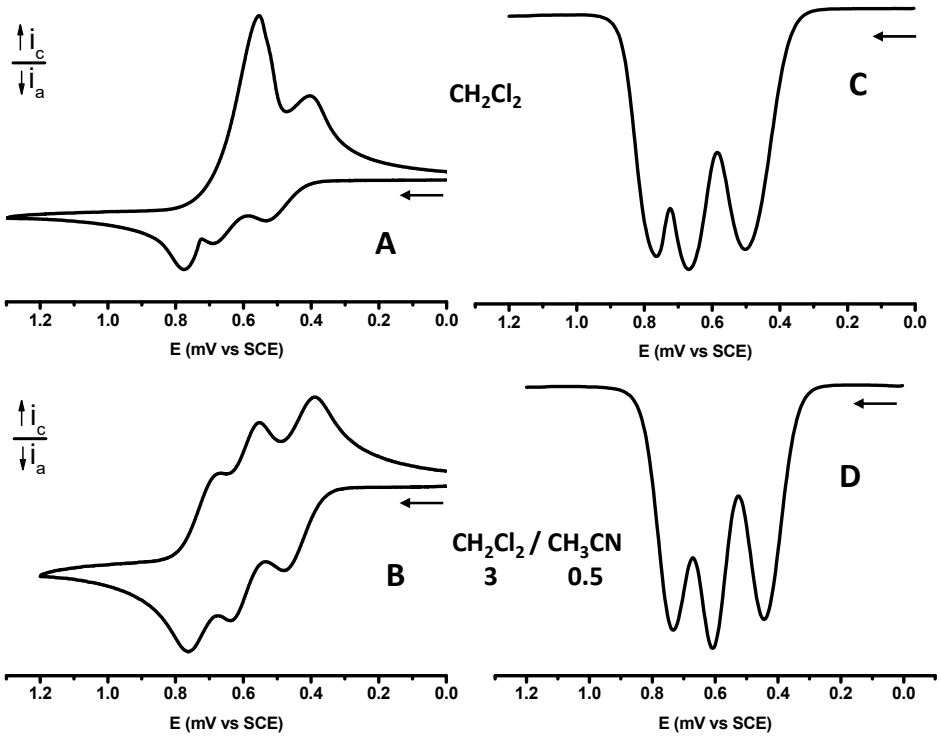

Figure S36. CV responses of dendron **3** (10^{-4} M) containing 0.1 M [*n*-Bu_4N][PF_6] recorded in: CH_2Cl_2 (A) and CH_2Cl_2/CH_3CN (3:05) (B). SWV responses of dendron **3** in CH_2Cl_2 (C) and CH_2Cl_2/CH_3CN (3:0.5) (D) with [*n*-Bu_4N][PF_6].

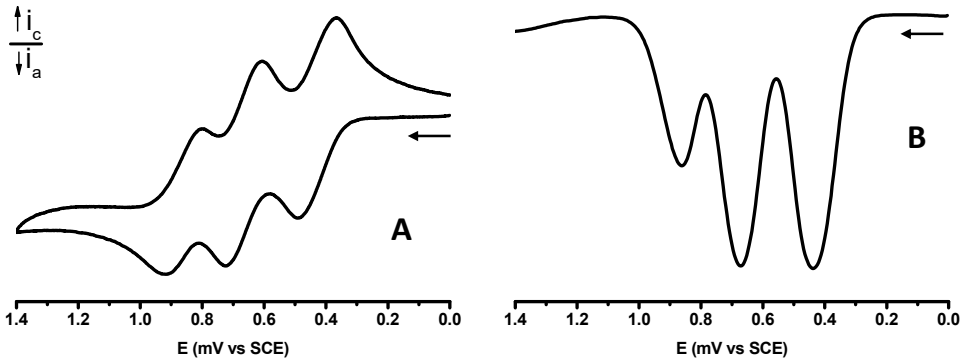

Figure S37. CV (A) and SWV (B) of dendron **3** (10^{-4} M) containing 0.1 M [*n*-Bu_4N][$B(C_6F_5)_4$] recorded in CH_2Cl_2.

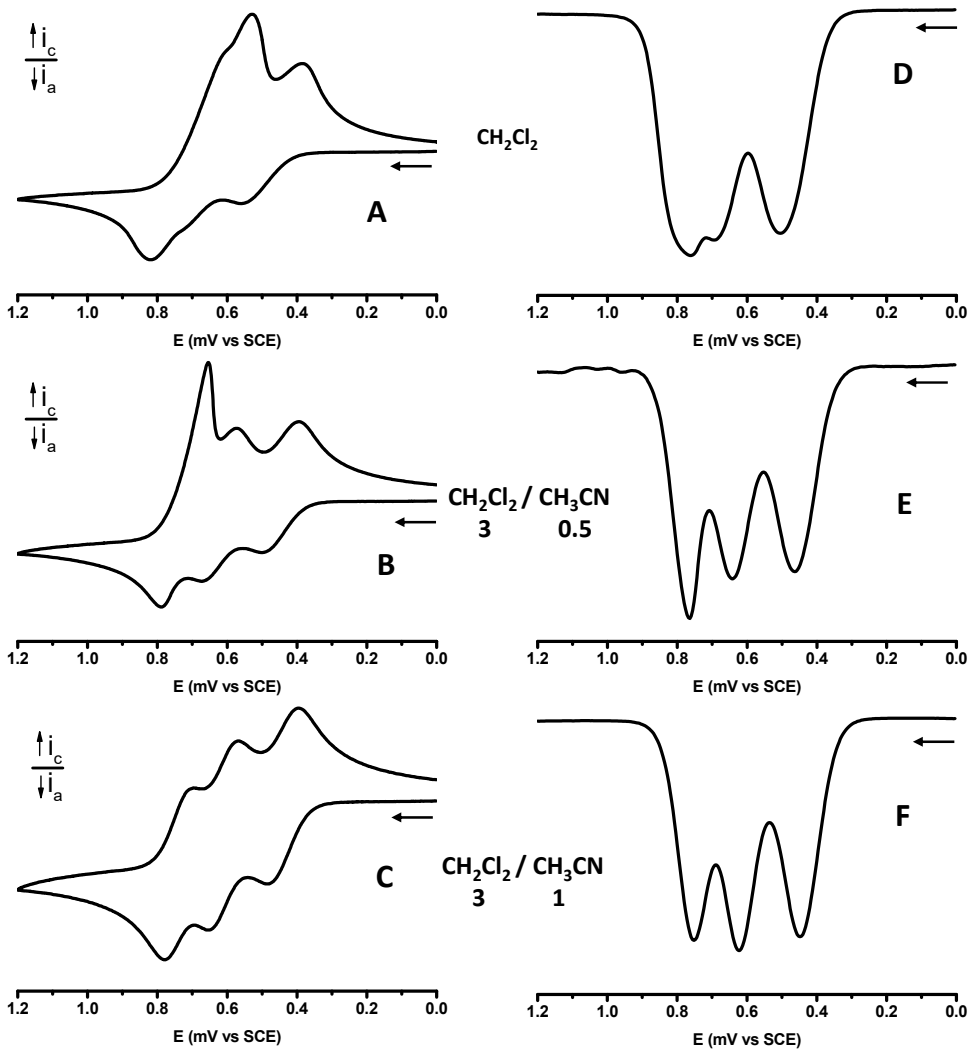

Figure S38. CV responses of dendrimer **4** (10^{-4} M) containing 0.1 M [*n*-Bu_4N][PF_6] recorded in: CH_2Cl_2 (A) , CH_2Cl_2/CH_3CN (3:05) (B) and CH_2Cl_2/CH_3CN (3:1) (C). SWV responses of dendrimer **4** in CH_2Cl_2 (D), CH_2Cl_2/CH_3CN (3:05) (E) and CH_2Cl_2/CH_3CN (3:1) (F) with [*n*-Bu_4N][PF_6].

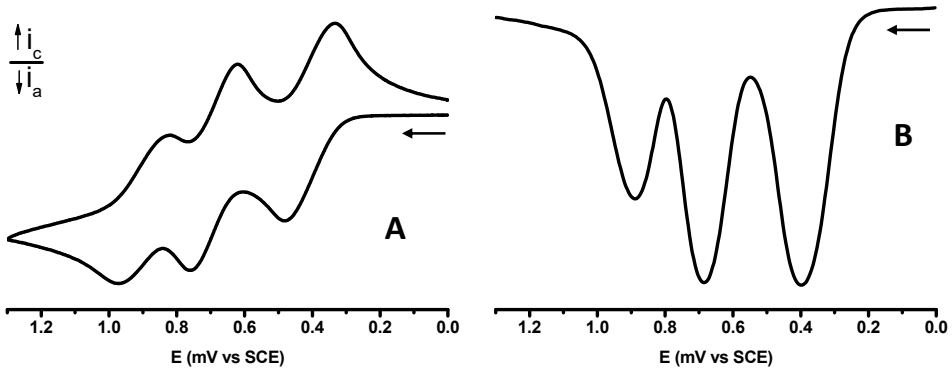

Figure S39. CV (A) and SWV (B) of dendrimer **4** (10^{-4} M) containing 0.1 M [*n*-Bu_4N][$B(C_6F_5)_4$] recorded in CH_2Cl_2.

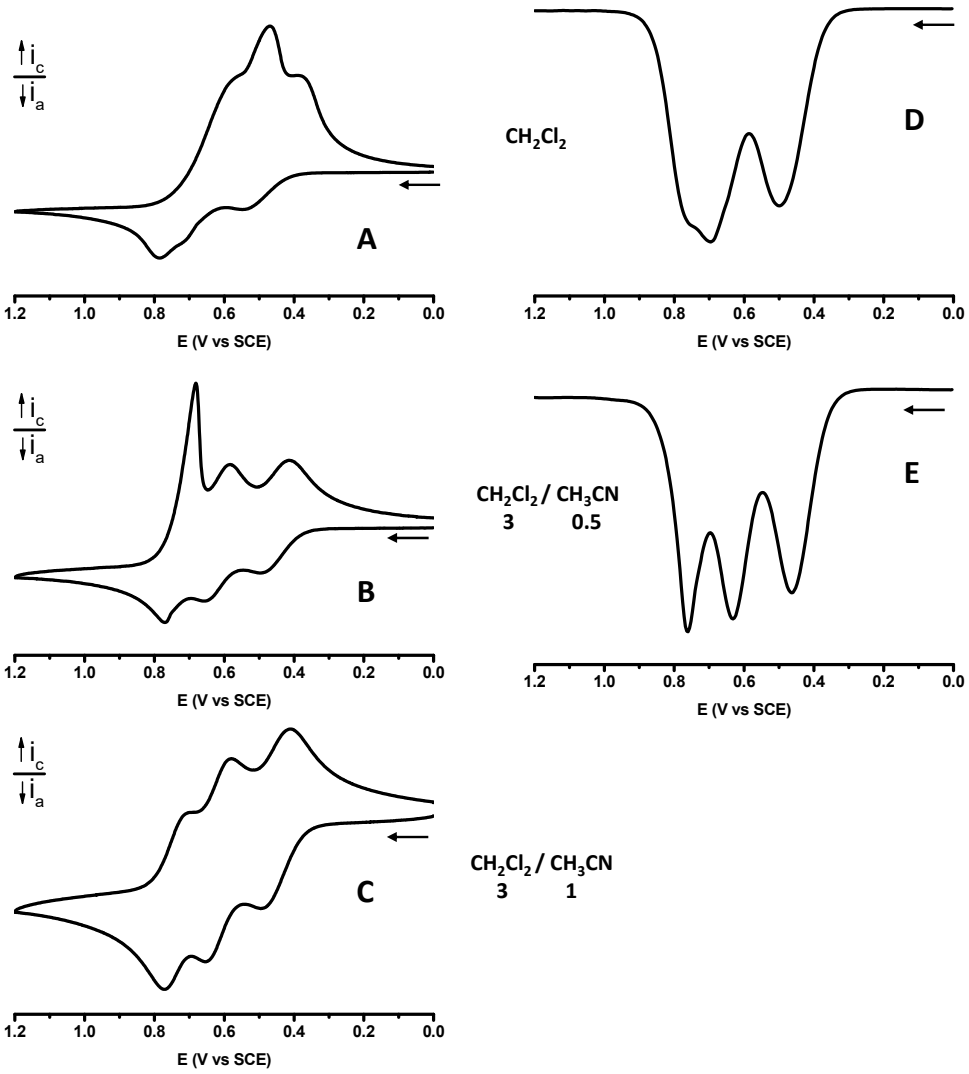

Figure S40. CV responses of dendrimer **5** (10^{-4} M) containing 0.1 M [*n*-Bu_4N][PF_6] recorded in: CH_2Cl_2 (A), CH_2Cl_2/CH_3CN (3:05) (B) and CH_2Cl_2/CH_3CN (3:1) (C). SWV responses of dendrimer **5** in CH_2Cl_2 (D) and CH_2Cl_2/CH_3CN (3:05) (E) with [*n*-Bu_4N][PF_6].

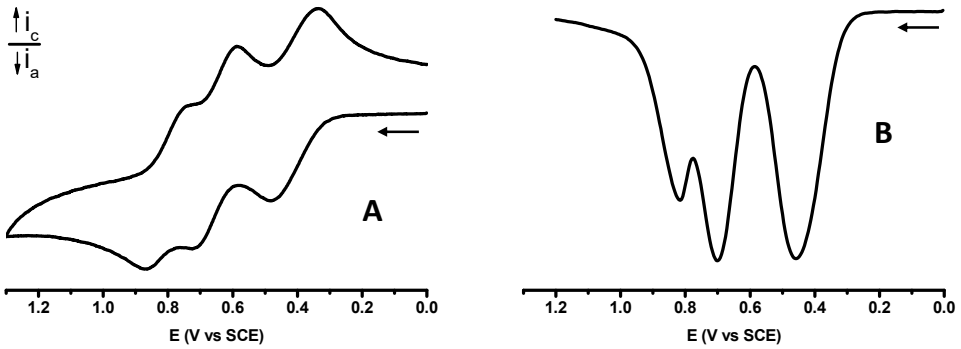

Figure S41. CV (A) and SWV (B) of dendrimer **5** (10^{-4} M) containing 0.1 M [*n*-Bu_4N][$B(C_6F_5)_4$] recorded in CH_2Cl_2.

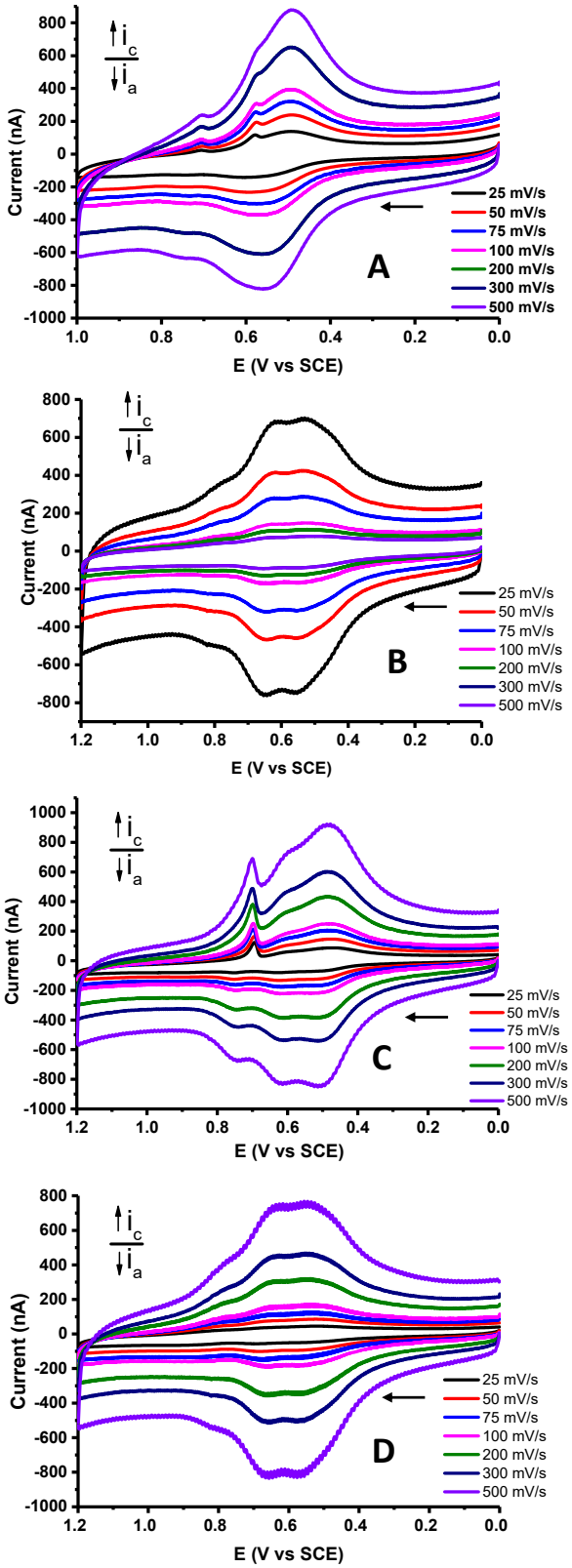

Figure S42. (A) CV responses at different scan rates of a Pt-disk electrode modified with films of dendrimer **5**: (A) after 10 successive scans and measured in 0.1M [*n*-Bu_4N][PF_6]/CH_2Cl_2 ($\Gamma \sim 4.19 \times 10^{-11}$ mol Fe/cm^2); (B) after 10 successive scans and measured in 0.1M [*n*-Bu_4N][$B(C_6F_5)_4$]/CH_2Cl_2 ($\Gamma \sim 4.10 \times 10^{-11}$ mol Fe/cm^2); (C) after 20 successive scans and measured in 0.1M [*n*-Bu_4N][PF_6]/CH_2Cl_2 ($\Gamma \sim 1.57 \times 10^{-10}$ mol Fe/cm^2); (D) after 20 successive scans and measured in 0.1M [*n*-Bu_4N][$B(C_6F_5)_4$]/CH_2Cl_2 ($\Gamma \sim 1.41 \times 10^{-10}$ mol Fe/cm^2).

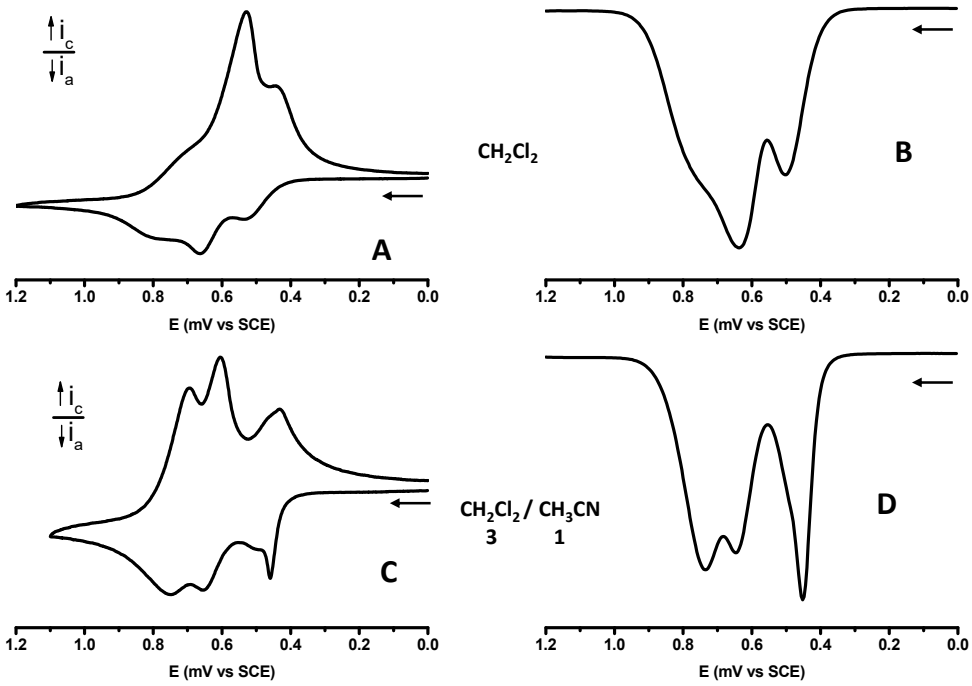

Figure S43. CV responses of polymers $\mathbf{7_n}$–$\mathbf{9_n}$ (10^{-4} M) containing 0.1 M [*n*-Bu_4N][PF_6] recorded in: CH_2Cl_2 (A) and CH_2Cl_2/CH_3CN (3:05) (B). SWV responses of polymers $\mathbf{7_n}$–$\mathbf{9_n}$ in CH_2Cl_2 (C) and CH_2Cl_2/CH_3CN (3:05) (D) with [*n*-Bu_4N][PF_6].

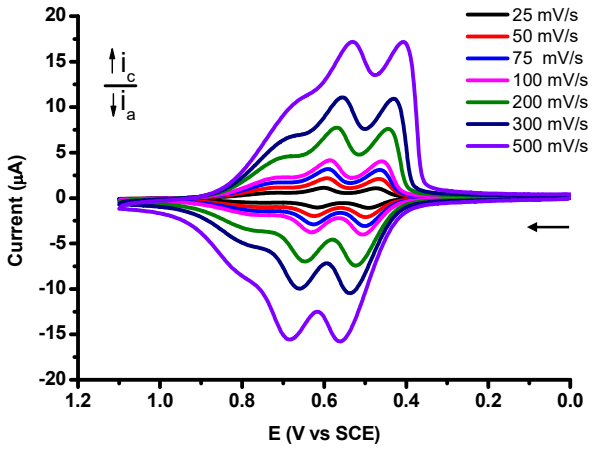

Figure S44. CV responses of a Pt-disk electrode modified with a film of polymers $\mathbf{7_n}$–$\mathbf{9_n}$ (10 successive scans and $\Gamma = 1.20 \times 10^{-9}$ mol Fe/cm^2) measured in 0.1M [*n*-Bu_4N][PF_6]/CH_2Cl_2 at different scan rates.